

Implicit Bias in Matrix Factorization and its Explicit Realization in a New Architecture

Yikun Hou¹, Suvrit Sra², and Alp Yurtsever³

^{1,3}Umeå University, Sweden

²Technical University of Munich, Germany

¹yikun.hou@umu.se

Abstract

Gradient descent for matrix factorization is known to exhibit an implicit bias toward approximately low-rank solutions. While existing theories often assume the boundedness of iterates, empirically the bias persists even with unbounded sequences. We thus hypothesize that implicit bias is driven by divergent dynamics markedly different from the convergent dynamics for data fitting. Using this perspective, we introduce a new factorization model: $X \approx UDV^\top$, where U and V are constrained within norm balls, while D is a diagonal factor allowing the model to span the entire search space. Our experiments reveal that this model exhibits a strong implicit bias regardless of initialization and step size, yielding truly (rather than approximately) low-rank solutions. Furthermore, drawing parallels between matrix factorization and neural networks, we propose a novel neural network model featuring constrained layers and diagonal components. This model achieves strong performance across various regression and classification tasks while finding low-rank solutions, resulting in efficient and lightweight networks.

1 Introduction

The Burer–Monteiro (BM) factorization (Burer & Monteiro, 2003) is a classical technique for obtaining low-rank solutions in optimization. It can be viewed as a simple neural network that uses a single layer of hidden neurons under linear activation. Indeed, say one has the factorization $X = UV^T$ where $U \in \mathbb{R}^{d \times r}$ and $V \in \mathbb{R}^{c \times r}$, then U and V can be thought of as the weights of the first and second layers, while r represents the number of hidden neurons. However, despite the similarity suggested by this view, there is a clear distinction between BM factorization and neural networks about how the rank r is chosen. In BM factorization, r is typically chosen to be small, close to the rank of the desired solution. Neural networks, on the other hand, often succeed even in overparametrized settings where r is large.

Recent findings of implicit regularization in matrix factorization narrows the gap between these two perspectives. For instance, in an effort to explain the empirical success of overparametrized neural networks, Gunasekar et al. (2017) demonstrate that gradient descent (with certain parameter selection) on BM factorization tends to converge toward approximately low-rank solutions even when $r = d$. Based on this observation, they conjecture that “*with small enough step sizes and initialization close enough to the origin, gradient descent on full-dimensional factorization converges to the minimum nuclear norm solution.*”

In a follow-up work, however, Razin & Cohen (2020) presented a counter-example demonstrating that implicit regularization in BM factorization cannot be explained by minimal nuclear norm, or in fact any norm. Specifically, they showed that there are instances where the gradient method applied to BM factorization yields a diverging sequence, and all norms thus grow toward infinity. Intriguingly, despite this divergence, they found that the rank of the estimate decreases toward its minimum.

Although this phenomenon might seem surprising initially, it is not uncommon for diverging sequences to follow a structured path. A prime example is the Power Method, the fundamental

algorithm for finding the largest eigenvalue and eigenvector pair of a matrix. Starting from a random initial point x_0 , the Power Method iteratively updates the estimate by multiplying it with the matrix. This process amplifies the component of the vector that aligns with the direction of the dominant eigenvector more than the other components, progressively leading x_k to align with this eigenvector. In practical implementations, x_k is scaled after each iteration to avoid numerical issues from divergence.

This perspective serves as the foundational motivation guiding our approach. Specifically, our key insight is that the implicit regularization in BM factorization (and neural networks) is driven by divergent dynamical behavior. This is markedly different from the standard (convergent) optimization dynamics helping with the data fitting. In this context, we hypothesize that these forces do not merely coexist but actively compete, influencing model behavior and performance in fundamentally conflicting ways. Our main goal in the development of this paper is to devise an approach that unravels these competing forces.

1.1 Overview of main contributions

- **A novel formulation for matrix factorization.** We model $X = UDV^\top$, where U and V are constrained within Frobenius norm balls. Projection onto this ball results in a scaling step similar to the Power Method. The middle term D is a diagonal matrix that allows the model to explore the entire search space despite U and V being bounded.

Empirically we demonstrate that the gradient method applied to the proposed formulation exhibits a pronounced implicit bias toward low-rank solutions. We compare our formulation against standard BM factorization with two unconstrained factors. Specifically, we investigate key factors such as step size and initialization, which prior work suggests might be contributing to implicit bias. We find that our factorization approach largely obviates the need to rely on these conditions: it consistently finds truly (rather than approximately) low-rank solutions across a wide range of initializations and step-sizes in our experiments. We believe these findings should be of broader interest to research on implicit bias.

- **A novel neural network architecture.** Motivated by the strong bias for low-rank solutions of the proposed factorization, we subsequently extend it to deep neural networks. Specifically, we do so by adding constrained layers and diagonal components. We demonstrate numerically that this constrained model performs on par with, or even better than, the standard architecture across various regression and classification tasks. Importantly, even here, our approach exhibits bias towards low-rank solutions, resulting in a natural pruning procedure to obtain compact, lightweight networks without compromising performance.

2 Related Work

Burer-Monteiro factorization. BM factorization is initially proposed for solving semi-definite programs (Burer & Monteiro, 2003, 2005; Boumal et al., 2016, 2020; Cifuentes, 2021) and is recognized for its efficiency in addressing low-rank matrix optimization problems, see (Sun & Luo, 2016; Bhojanapalli et al., 2016; Park et al., 2017, 2018; Hsieh et al., 2018; Sahin et al., 2019; Lee et al., 2022; Yalçın et al., 2023) and the references therein. Building on the connections between training problems for (non-linear) two-layer neural networks and convex (copositive) formulations (see (Pilanci & Ergen, 2020; Ergen & Pilanci, 2020; Sahiner et al., 2021) and the references therein), Sahiner et al. (2023) recently introduced BM factorization to solve convex formulations for various neural network architectures, including fully connected networks with ReLU and gated ReLU (Fiat et al., 2019) activations, two-layer convolutional neural networks (LeCun et al., 1989a), and self-attention mechanisms based on transformers (Vaswani et al., 2017).

Implicit regularization. While neural network-based systems are rapidly emerging as a dominant technology, the mechanisms underlying their generalization capabilities are yet to be fully understood. One promising line of research aims to explain this success through the concept of ‘implicit regularization,’ which is induced by the optimization methods and formulations used

during neural network training (Neyshabur et al., 2014, 2017; Neyshabur, 2017). Several studies have explored matrix factorization to investigate implicit bias in linear neural networks (Gunasekar et al., 2017; Arora et al., 2018; Razin & Cohen, 2020; Belabbas, 2020; Li et al., 2021). Le & Jegelka (2022) extended these results to the final linear layers of nonlinear ReLU-activated feedforward networks with fully connected layers and skip connections. More recently Timor et al. (2023) investigated implicit regularization in ReLU networks. Much of the existing work focuses on gradient flow dynamics in the limit of infinitesimal learning rates. In particular, Gidel et al. (2019) examined discrete gradient dynamics in two-layer linear neural networks, showing that the dynamics progressively learn solutions of reduced-rank regression with a gradually increasing rank.

Constrained neural networks. Regularizers are frequently used in neural network training to prevent overfitting and improve generalization (Goodfellow et al., 2016), or to achieve structural benefits such as sparse and compact network architectures (Scardapane et al., 2017). However, it is conventional to apply these regularizers as penalty functions in the objective rather than as hard constraints, addressing them within gradient-based optimization via their (sub)gradients. This approach is likely favored due to the ease of implementation, as pre-built functions are readily available in common neural network packages. Several independent studies have also applied proximal methods across different networks and applications, finding that proximal-based methods tend to yield solutions with more pronounced structures (Bai et al., 2019; Yang et al., 2020; Yun et al., 2021; Yurtsever et al., 2021; Yang et al., 2022). Structural regularization in the form of hard constraints, however, appears to be rare in neural network training. One notable exception is in the context of neural network training with the Frank-Wolfe algorithm (Pokutta et al., 2020; Zimmer et al., 2022; Macdonald et al., 2022), where constraints are necessary due to the algorithm’s requirement for a bounded domain.

There are other use cases of constraints in neural networks. For instance, constraints can be applied to ensure adherence to real-world conditions in applications where they are necessary (Pathak et al., 2015; Márquez-Neila et al., 2017; Jia et al., 2017; Kervadec et al., 2019; Weber et al., 2021), or to incorporate physical laws in physics-informed neural networks (Raissi et al., 2019; Lu et al., 2021; Patel et al., 2022). In these cases, the feasible set is typically complex and difficult to project onto; therefore, optimization algorithms like primal-dual methods or augmented Lagrangian techniques are used. Constraints are also present in lifted neural networks, a framework where the training problem is reformulated in a higher-dimensional ‘lifted’ space. In this space, conventional activation functions like ReLU, used in the original formulation, are expressed as constraints (Askari et al., 2018; Sahiner et al., 2021; Bartan & Pilanci, 2021; Prakhya et al., 2024).

Pruning. Neural networks are often trained in an over-parameterized regime to enhance generalization and avoid getting stuck in poor local minima. However, these models can suffer from excessive memory and computational resource demands, making them less efficient for deployment in real-world applications (Chang et al., 2021). Several compression techniques have been studied in the literature, including parameter quantization (Krishnamoorthi, 2018), knowledge distillation (Gou et al., 2021), and pruning.

Pruning reduces the number of parameters, resulting in more compact and efficient models that are easier to deploy. The literature on pruning is extensive, with diverse methods proposed with distinct characteristics. Various criteria are used to determine which weights to prune, including second-order derivative-based methods (LeCun et al., 1989b; Hassibi & Stork, 1992), magnitude-based pruning (Janowsky, 1989; Han et al., 2015), saliency heuristics (Mozer & Smolensky, 1988; Lee et al., 2018), and matrix or tensor factorization-based techniques (Xue et al., 2013; Sainath et al., 2013; Jaderberg et al., 2014; Lebedev et al., 2015; Swaminathan et al., 2020), among others. A comprehensive review of pruning methods is beyond the scope of this paper due to space limitations and the diversity of approaches. For more detailed reviews, we refer to (Reed, 1993; Blalock et al., 2020; Cheng et al., 2024), and the references therein.

3 Matrix Factorization with a Diagonal Component

Consider the *matrix sensing* problem, where the goal is to recover a *positive semidefinite* (PSD) matrix $X \in \mathbb{S}_+^{d \times d}$ from a set of linear measurements $b = \mathcal{A}(X) \in \mathbb{R}^n$. We define $\mathcal{A} : \mathbb{R}^{d \times d} \rightarrow \mathbb{R}^n$ through symmetric measurement matrices $A_1, \dots, A_n \in \mathbb{S}^{d \times d}$, such that $\mathcal{A}(X) = [\langle A_1, X \rangle \cdots \langle A_n, X \rangle]^\top$ and $\mathcal{A}^\top y = \sum_{i=1}^n y_i A_i$. We particularly focus on the data-scarce setting where $n \ll d^2$. A popular example is the matrix completion problem, where the goal is to reconstruct a matrix X from a subset of its entries. This problem is inherently under-determined; however, successful recovery is possible if X is known to be low-rank (Candes & Recht, 2012).

Remark 1. We focus on the recovery problem of a PSD matrix for simplicity; note that a non-square matrix sensing problem can also be reformulated as a PSD matrix sensing problem through a simple transformation (Park et al., 2017).

The problem described above can be cast as the following rank-constrained optimization problem:

$$\min_{X \in \mathbb{S}_+^{d \times d}} f(X) := \frac{1}{2} \|\mathcal{A}(X) - b\|_2^2 \quad \text{subj. to} \quad \text{rank}(X) \leq r. \quad (1)$$

Although rank-constrained matrix optimization problems are typically NP-hard, various methods have been developed to provide practical approximations. Examples include hard thresholding algorithms (Jain et al., 2010; Goldfarb & Ma, 2011; Kyrillidis & Cevher, 2014), convex relaxation techniques (Candes & Recht, 2012; Recht et al., 2010), and BM factorization (Burer & Monteiro, 2003; Sun & Luo, 2016; Bhojanapalli et al., 2016; Park et al., 2017).

The main idea behind BM factorization is to reparametrize the decision variable X as UU^\top , where the factor $U \in \mathbb{R}^{d \times r}$, and r is a positive integer that controls the rank of the resulting product. Problem (1) can then be reformulated as:

$$\min_{U \in \mathbb{R}^{d \times r}} \frac{1}{2} \|\mathcal{A}(UU^\top) - b\|_2^2. \quad (2)$$

Despite the fact that finding the global minimum of (2) remains challenging, a local solution can be approximated using the gradient method (Lee et al., 2016). Initializing at $U_0 \in \mathbb{R}^{d \times r}$, perform the iteration:

$$U_{k+1} = U_k - \eta \nabla_U f(U_k U_k^\top), \quad (3)$$

where $\eta > 0$ is the step-size, and the gradient $\nabla_U f$ is computed as

$$\nabla_U f(UU^\top) = 2 \nabla f(UU^\top) U = 2 \mathcal{A}^\top (\mathcal{A}(UU^\top) - b) U.$$

Selecting the factorization rank r is a critical decision that might impact the solution. A small r may lead to spurious local minima, resulting in inaccurate outcomes (Waldspurger & Waters, 2020). Conversely, a large r might weaken rank regularization, rendering the problem underdetermined. Conventional wisdom in BM factorization suggests finding a moderate choice that balances these two extremes. However, a key observation in (Gunasekar et al., 2017) is that the gradient method applied to (2) exhibits a tendency towards approximately low-rank solutions (*i.e.*, a decaying singular value spectrum) even when $r = d$. Below, we restate their conjecture:

Conjecture in (Gunasekar et al., 2017). Suppose gradient flow (*i.e.*, gradient descent with an infinitesimally small step-size) is initialized at a *full-rank matrix arbitrarily close to the origin*. If the limit of the gradient flow, $X_{\text{GF}} = UU^\top$, exists and is a global optimum of (1) with $\mathcal{A}(X_{\text{GF}}) = b$, then X_{GF} is the minimal nuclear-norm solution to (1).

Remark 2. This conjecture outlines three conditions for implicit bias: a small step-size, near-origin full-rank initialization, and consistent measurements (\mathcal{A}, b) . However, these conditions are often unconventional. For example, small step-sizes are typically avoided because they slow down convergence. Similarly, near-origin initialization is counterintuitive, as the origin is a trivial spurious stationary point of (2).

3.1 The Proposed Factorization

We propose reparameterizing $X = UDU^\top$, where $U \in \mathbb{R}^{d \times r}$ is constrained to have a bounded norm, and $D \in \mathbb{R}^{r \times r}$ is a non-negative diagonal matrix:

$$\min_{\substack{U \in \mathbb{R}^{d \times r} \\ D \in \mathbb{R}^{r \times r}}} \frac{1}{2} \|\mathcal{A}(UDU^\top) - b\|_2^2 \quad \text{s.t.} \quad \|U\|_F \leq \alpha, \quad D_{ii} \geq 0, \quad D_{ij} = 0, \quad \forall i \text{ and } \forall j \neq i, \quad (4)$$

where $\alpha > 0$ is a model parameter. When the problem is well-scaled, for instance through basic preprocessing with data normalization, we found that $\alpha = 1$ is a reasonable choice.

Placing in multiple factors and with constraints, we perform projected-gradient updates on U and D with step-size $\eta > 0$:

$$\begin{aligned} U_{k+1} &= \Pi_U (U_k - \eta \nabla_U f(U_k D_k U_k^\top)) \\ D_{k+1} &= \Pi_D (D_k - \eta \nabla_D f(U_k D_k U_k^\top)), \end{aligned} \quad (5)$$

where Π_U and Π_D are projections for the constraints in (4); while the gradients are

$$\begin{aligned} \nabla_U f(UDU^\top) &= 2 \nabla f(UDU^\top) U D, \\ \nabla_D f(UDU^\top) &= U^\top \nabla f(UDU^\top) U. \end{aligned}$$

3.2 Numerical Experiments on Matrix Factorization

We present numerical experiments comparing the empirical performance of the proposed approach with the classical BM factorization. Specifically, we examine the impact of initialization and step-size on the singular value spectrum of the resulting solution.

We set up a synthetic matrix completion problem to recover a PSD matrix $X_{\natural} = U_{\natural} U_{\natural}^\top$, where the entries of $U_{\natural} \in \mathbb{R}^{100 \times 3}$ are independently and identically (*iid*) drawn from the standard Gaussian distribution. We randomly sample $n = 900$ entries of X_{\natural} and store them in the vector $b \in \mathbb{R}^n$. The goal is to recover X_{\natural} from b by solving problems (2) and (4). For initialization, we generate $U_0 \in \mathbb{R}^{d \times d}$ with entries drawn *iid* from standard Gaussian distribution and rescale it to have the Frobenius norm $\xi > 0$ (we investigate the impact of ξ). We initiate D_0 from the identity matrix.

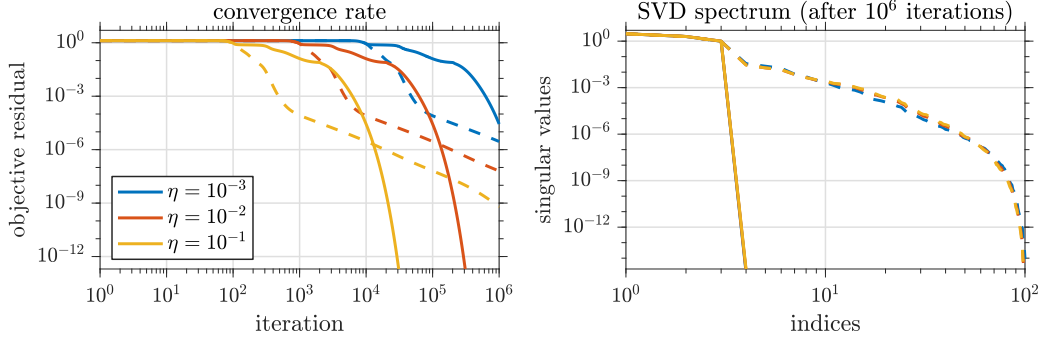
The results are shown in [Figure 1](#). First, we examine the impact of step-size. To this end, we fix $\xi = 10^{-2}$ and test different values of η . In the left panel, we plot the objective residual as a function of iterations. As expected, we observe that a smaller step-size slows down convergence. In the right panel, we plot the singular value spectrum of the results attained after 10^6 iterations. We observe no direct connection between step-size and implicit bias in BM factorization.

Next, we investigate the impact of initialization. We fix the step-size at $\eta = 10^{-2}$ and evaluate the effect of varying ξ . We observe a correlation between the implicit bias of the BM factorization and ξ , which determines the initial distance from the origin. Initializing closer to the origin in the classical BM factorization yields solutions with a faster spectral decay. Notably, the UDU factorization demonstrates a strong implicit bias toward truly low-rank solutions, regardless of the choice of η or ξ .

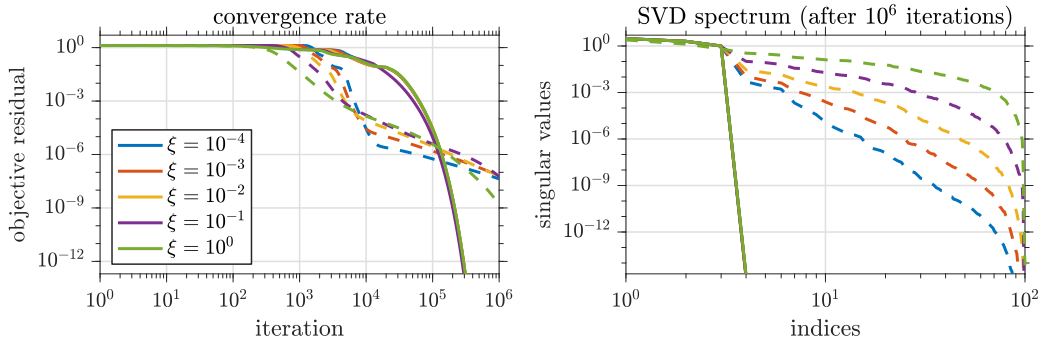
We provide additional experiments on matrix factorization problems in the Appendices. Specifically, [Appendix A.1](#) considers the matrix completion problem with noisy measurements, where b is perturbed with Gaussian noise. The results remain consistent with the noiseless case: the UDU model exhibits an implicit bias toward truly low-rank solutions, while the classical BM factorization yields approximately low-rank solutions, with spectral decay strongly influenced by initialization.

In [Appendix A.2](#), we present the evolution of the factors U and D over the iterations. Interestingly, the UDU model produces rank-revealing solutions, with the columns of U converging to zero in certain directions. Specifically, U tends to grow along certain directions, while the rescaling induced by projection onto the bounded constraint shrinks other coordinates. This behavior aligns with the mechanism of the power method and offers insights into its connection with divergent forces.

Additionally, we present numerical experiments on a matrix sensing problem arising in phase retrieval image recovery in [Appendix A.3](#). As before, the UDU framework consistently promotes low-rank solutions, and this structural bias significantly enhances the quality of the recovered image, as demonstrated by our results.



Impact of **step-size** (η), in **noiseless** setting, with fixed initialization.



Impact of **initial distance to origin** (ξ), in **noiseless** setting, with fixed step-size.

Figure 1: Impact of step-size and initialization on implicit bias. **Solid lines represent our UDU factorization**, while **dashed lines denote the classical BM factorization**. [Left] Objective residual vs. iterations. [Right] Singular value spectrum after 10^6 iterations. In all cases, UDU produces truly low-rank solutions, whereas the classical approach results in approximate low-rank structures.

4 Feedforward Neural Networks with Diagonal Hidden Layers

This section extends our approach to neural networks. Consider a dataset comprising n data points $(\mathbf{x}_i, \mathbf{y}_i) \in \mathbb{R}^d \times \mathbb{R}^c$. We first define a three-layer neural network defined as

$$\phi(\mathbf{x}) := \sum_{j=1}^m \mathbf{v}_j w_j \mathbf{u}_j^\top \mathbf{x} \approx \mathbf{y}. \quad (6)$$

The first and third layers are fully connected, and the middle is a diagonal layer, as illustrated in Figure 2. Drawing parallels between our matrix factorization model in (4) and neural network training, we impose Euclidean norm constraints on the weights of the fully connected layers. Under these conditions, the training problem can be formulated as follows:

$$\begin{aligned} \min_{\substack{\mathbf{u}_j \in \mathbb{R}^d \\ \mathbf{v}_j \in \mathbb{R}^c \\ w_j \in \mathbb{R}}} & \frac{1}{2n} \sum_{i=1}^n \left\| \sum_{j=1}^m \mathbf{v}_j w_j \mathbf{u}_j^\top \mathbf{x}_i - \mathbf{y}_i \right\|_2^2 \\ \text{subj.to} & \sum_{j=1}^m \|\mathbf{u}_j\|_2^2 \leq 1, \quad \sum_{j=1}^m \|\mathbf{v}_j\|_2^2 \leq 1, \quad \text{and} \quad w_j \geq 0; \quad \text{for all } j = 1, \dots, m. \end{aligned} \quad (7)$$

The norm constraints in our training problem can be interpreted as a stronger form of weight decay, one of the most commonly used regularization techniques in neural networks, which lends further justification to our formulation. We refer to this neural network structure as UDV.

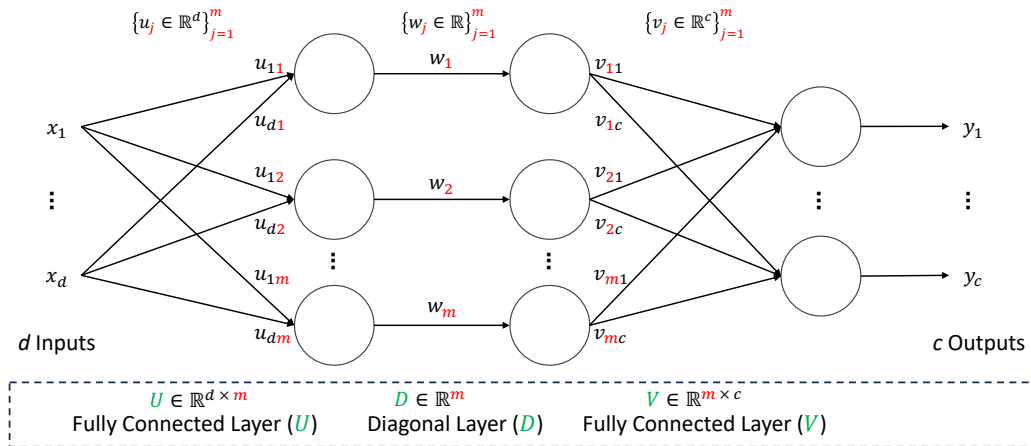


Figure 2: UDV structure. The weights in diagonal layer D are denoted as w_j .

4.1 Numerical Experiments on Neural Networks

In this section, we test the proposed UDV framework on regression and classification tasks, comparing it with fully connected two-layer neural networks (denoted as UV in the subsequent text) using both linear and ReLU activation functions. This comparison is fair in terms of computational cost, as the cost incurred by the diagonal layer—which can also be viewed as a parameterized linear activation function—is negligible. We demonstrate a strong empirical bias toward low-rank solutions in all our experiments. We also present a proof-of-concept use case of this strong bias, combined with an SVD-based pruning strategy, to produce compact networks.

4.1.1 Implementation Details

Computing environment. All classification tasks were conducted on an NVIDIA A100 GPU with four cores of the AMD Epyc 7742 processor, while regression tasks were conducted on a single core of an Intel Xeon Gold 6132 processor. We used Python 3.9.5 and PyTorch 2.0.1.

Datasets. We used two datasets for the regression tasks: House Prices - Advanced Regression Techniques (HPART) (Anna Montoya, 2016) and New York City Taxi Trip Duration (NYCTTD) (Risdal, 2017). We allocated 80% of the data for the training and reserved the remaining 20% for validation. Following (Huang, 2003), we set the number of hidden neurons in the diagonal layer $m = \text{round}(\sqrt{(c+2)d} + 2\sqrt{d/(c+2)})$. This results in a network structure $(d-m-c)$ of 79-26-1 for HPART, and 12-10-1 for NYCTTD.

For classification tasks, we used the normalized MNIST dataset (LeCun et al., 2010). We applied transfer learning by replacing the classifier layers of three advanced neural networks –MaxViT-T (Tu et al., 2022), EfficientNet-B0 (Tan & Le, 2019), and RegNetX-32GF (Radosavovic et al., 2020)– with UDV, while using pre-trained weights from ImageNet-1K (Deng et al., 2009). Specifically, we retained all layers up to the first fully connected layer of the classifier and replaced the subsequent layers. The number of hidden neurons in the diagonal layer was set to as $m = \text{floor}(\frac{2}{3}d)$. This results in a UDV network structure $(d-m-c)$ of 512-341-10 for MaxViT-T, 1280-853-10 for EfficientNet-B0, and 2520-1680-10 for RegNetX-32GF.

Loss function. We used mean squared error for regression and cross-entropy loss for classification.

Optimization methods. We tested the results using four different optimization algorithms for training: Adam (Kingma & Ba, 2014), Mini-Batch Gradient Descent (MBGD) (LeCun et al., 2002), NAdam (Dozat, 2016), and Mini-Batch Gradient Descent with Momentum (MBGDM) (Sutskever et al., 2013). For classification, we used different batch sizes for different models: 128 for MaxViT-T and RegNetX-32GF, and 384 for EfficientNet-B0.

Table 1: Model performance using different models. M, E, and R represent the transferred models MaxVit-T, EfficientNet-B0, and RegNetX-32GF, respectively.

Tasks	Regression (Test Loss)		Classification (Test Accuracy)		
Dataset	HPART	NYCTTD	MNIST		
UDV	1.304×10^{-3}	5.248×10^{-6}	M: 99.67%	E: 99.63%	R: 99.74%
	Adam: 10^{-3}	NAdam: 10^{-4}	MBGDM: 10^{-2}	MBGDM: 10^{-1}	MBGDM: 10^{-2}
UV	1.333×10^{-3}	5.251×10^{-6}	M: 99.69%	E: 99.60%	R: 99.66%
	Adam: 10^{-3}	Adam: 10^{-3}	MBGDM: 10^{-2}	Adam: 10^{-3}	MBGD: 10^0
UV-ReLU	1.167×10^{-3}	5.323×10^{-6}	M: 99.68%	E: 99.68%	R: 99.73%
	Adam: 10^{-3}	NAdam: 10^{-3}	NAdam: 10^{-4}	MBGDM: 10^{-1}	MBGD: 10^0

We tuned the step size for all models and optimization algorithms: For regression tasks, we tested step sizes 10^{-4} , 10^{-3} , 10^{-2} , 10^{-1} , 1, 2, 3. Larger step sizes (1, 2, 3) were often excluded for the UV model due to divergence. In classification experiments, we tested learning rates 10^{-6} , 10^{-5} , 10^{-4} , 10^{-3} , 10^{-2} , 10^{-1} , 1 with Adam and NAdam; and we tested 10^{-3} , 10^{-2} , 10^{-1} , 1, 2, 3, 5 with MBGD and MBGDM.

Training Procedure. UV and UDV models were initialized identically, with the diagonal elements of D initialized using Kaiming Uniform Initialization, consistent with the default initialization for fully connected layers in PyTorch. The models were trained for 200 epochs on HPART, 50 epochs on NYCTTD, and 70 epochs on MNIST; and results were averaged over 1000 random seeds for HPART, 100 for NYCTTD, and 1 for MNIST to ensure robustness. The validation loss, used as a generalization metric in regression, was averaged over the final 20 epochs for the HPART dataset and the final 5 epochs for the NYCTTD dataset. Similarly, validation accuracy for classification tasks was averaged over the last 5 epochs to ensure stability in the reported values.

Repository. The code is available at <https://github.com/Titanium-H/UDV>

4.1.2 Low-rank Bias in Neural Network Training

Table 1 presents the validation loss (for regression) or validation accuracy (for classification) of the UDV model compared to the classical UV model with linear and ReLU activation functions. For each configuration (dataset and model architecture), the results are obtained by selecting the best algorithm and learning rate pair. Moreover, Figure 3 illustrates the singular value spectrum of the solutions corresponding to each entry in these tables. We focus on the singular values from the U and UD layers, as they generate the primary data representation, while omitting the V layer, which serves as the feature selection layer and is a tall matrix by definition, given that $c \ll m$ in most cases. Collectively, these results show that the UDV framework achieves competitive prediction accuracy while exhibiting a strong implicit bias toward low-rank solutions, as indicated by the faster decay in the singular value spectrum.

4.1.3 Reducing Network Size with SVD-based Pruning

Efficient and lightweight feed-forward layers are crucial for real-world applications. For instance, the Apple Intelligence Foundation Models (Gunter et al., 2024) recently reported that pruning hidden dimensions in feed-forward layers yields the most significant gains in their foundation models. Building on this insight, we leverage the inherent low-rank bias of the UDV architecture through an SVD-based pruning strategy to produce compact networks without sacrificing performance.

A low-rank solution was observed when applying SVD to UD layers:

$$UD = USV^\top, \quad \mathbf{U} \in \mathbb{R}^{d \times m}, \quad \mathbf{S} \in \mathbb{R}^{m \times m}, \quad \mathbf{V}^\top \in \mathbb{R}^{m \times m}. \quad (8)$$

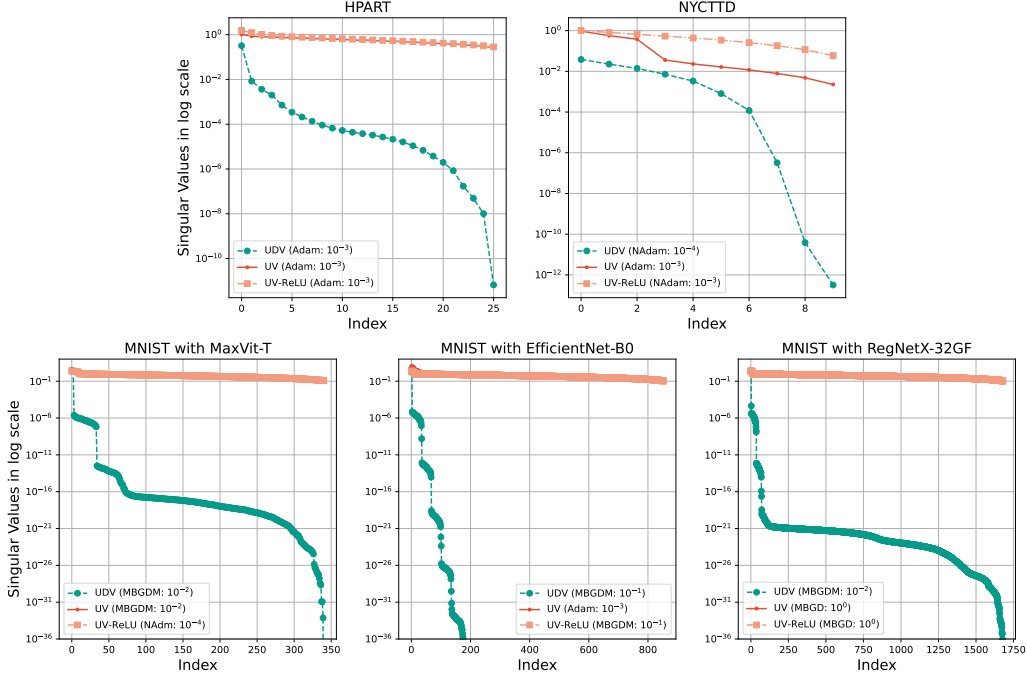


Figure 3: Singular value spectrum corresponding to the solutions reported in Table 1.

By dropping small singular values in \mathbf{S} , these matrices can be truncated to $\bar{\mathbf{U}} \in \mathbb{R}^{d \times r}$, $\bar{\mathbf{S}} \in \mathbb{R}^{r \times r}$ and $\bar{\mathbf{V}}^T \in \mathbb{R}^{r \times m}$, where $0 < r < m$. Consequently, $(m - r)$ neurons can be pruned, and new weight matrices are assigned:

$$\bar{\mathbf{U}} = \bar{\mathbf{U}} \in \mathbb{R}^{d \times r}, \quad \bar{\mathbf{D}} = \bar{\mathbf{S}} \in \mathbb{R}^{r \times r}, \quad \bar{\mathbf{V}} = \bar{\mathbf{V}}^T \mathbf{V} \in \mathbb{R}^{r \times c}. \quad (9)$$

We applied this pruning strategy on the models from Table 1. The left part of Figure 4 presents an example comparing the generalization capability of pruned models. For comparison, we created compact models by training from scratch with a reduced number of neurons m in the hidden layer. The performance change for these models is shown in the right panel of Figure 4. Although our pruned networks derived from UDV demonstrate that models with significantly fewer parameters can still achieve strong generalization, these compressed architectures are often more challenging to optimize directly within the reduced space, consistent with prior findings in the literature (Arora et al., 2018; Chang et al., 2021). We omit the results for retraining with the UV model, as they show similar trends to UDV in this context, though UDV generally exhibits superior generalization.

4.1.4 Further Details and Discussions

Our findings in experiments on neural networks align with the results observed in matrix factorization. A key distinction, however, was the use of different optimization algorithms, including stochastic gradients and momentum steps, in neural network experiments. Despite these differences, the UDV architecture consistently demonstrated a strong bias toward low-rank solutions. Additional experiments and details can be found in the Appendices, with key results summarized below:

- In the early stages of this research, we explored four variants of UDV, each differing slightly in their constraints. We selected the version presented in (7), as it generally exhibits the most pronounced decay in the singular value spectrum. For completeness, details of the other three variants are provided in Appendix B.1.
- Appendix B.2 provides additional results for the experiment described in Section 4.1.2. Specifically, we present results analogous to those in Table 1 and Figure 3, but focusing exclusively on the MBGDM algorithm. These results exhibit similar trends, reinforcing consistency across different methods. Additionally, comprehensive performance comparisons across all algorithms and models are provided in Tables SM2 to SM5 in the Appendices.

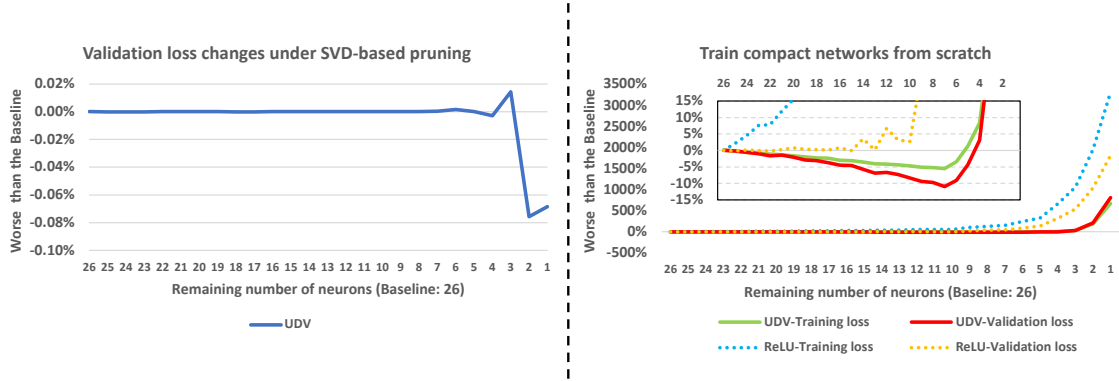


Figure 4: Comparison of SVD-based pruning and re-training compact networks on the HPART dataset using the NAdam algorithm with a learning rate of 10^{-3} . Negative percentages indicate improvements over the baseline. SVD-based pruning demonstrates that the UDV leads to a compact model without performance degradation, while retraining shows that the UDV achieves better generalization in a compact model.

- Additional results on SVD-based pruning are provided in [Appendix B.3](#). We demonstrate that the UDV framework consistently achieves low-rank solutions across various problem configurations. Furthermore, we analyze the effect of learning rate on the singular value spectrum, similar to the analysis in [Figure 1](#), but applied to neural network experiments. This analysis confirms that the UDV framework produces low-rank solutions across a broad range of learning rates.
- [Appendix B.4](#) extends the UDV framework by incorporating ReLU activation. Preliminary experiments with the UDV-ReLU model indicate that it also tends to yield low-rank solutions, similar to those observed in the original UDV framework.
- Prior work on implicit bias in neural networks suggests that increasing depth enhances the tendency toward low-rank solutions ([Arora et al., 2019](#); [Feng et al., 2022](#)), raising the question of whether the pronounced bias in the UDV framework is just a consequence of adding a diagonal layer. To investigate this, we conducted experiments comparing the UDV model to fully connected three-layer networks, as detailed in [Appendix B.5](#). Additionally, we included a UDV model without constraints in these comparisons. The results indicate that this bias cannot be attributed solely to depth, highlighting the critical role of explicit constraints.
- [Appendix B.6](#) compares the spectral decay of the UDV network to that induced by classical weight decay regularization in two- and three-layer networks. The results show that while weight decay promotes singular value decay, it can not reproduce the strong decay observed in the UDV model.

5 Conclusions

We proposed a new matrix factorization framework, inspired by the observation that implicit bias is driven by dynamics—potentially divergent—that are distinct from those leading to convergence of the objective function. This framework constrains the factors within Euclidean norm balls and introduces a middle diagonal factor to ensure the search space is not restricted. Numerical experiments demonstrate that this approach significantly strengthens the low-rank bias in the solution.

To explore the broader applicability of our findings, we designed an analogous neural network architecture with three layers, constraining the fully connected layers and adding a diagonal hidden layer, referred to as UDV. Extensive experiments show that the proposed UDV architecture achieves competitive performance compared to standard fully connected networks, while inducing a structured solution with a strong bias toward low-rank representations. Additionally, we explored the utility of this low-rank structure by applying an SVD-based pruning strategy, illustrating how it can be leveraged to construct compact networks that are more efficient for downstream tasks.

Acknowledgments

Alp Yurtsever and Yikun Hou were supported by the Wallenberg AI, Autonomous Systems and Software Program (WASP) funded by the Knut and Alice Wallenberg Foundation. Part of computations were enabled by the Berzelius resource provided by the Knut and Alice Wallenberg Foundation at the National Supercomputer Centre. Another part of computations were conducted using the resources of High Performance Computing Center North (HPC2N) which is mainly funded by The Kempe Foundations and the Knut and Alice Wallenberg Foundation. Suvrit Sra acknowledges generous support from the Alexander von Humboldt (AvH) foundation.

References

- DataCanary Anna Montoya. House prices - advanced regression techniques, 2016. URL <https://kaggle.com/competitions/house-prices-advanced-regression-techniques>.
- Sanjeev Arora, Rong Ge, Behnam Neyshabur, and Yi Zhang. Stronger generalization bounds for deep nets via a compression approach. In *International conference on machine learning*, pp. 254–263. PMLR, 2018.
- Sanjeev Arora, Nadav Cohen, Wei Hu, and Yuping Luo. Implicit regularization in deep matrix factorization. *Advances in Neural Information Processing Systems*, 32, 2019.
- Armin Askari, Geoffrey Negiar, Rajiv Sambharya, and Laurent El Ghaoui. Lifted neural networks. *arXiv preprint arXiv:1805.01532*, 2018.
- Yu Bai, Yu-Xiang Wang, and Edo Liberty. Proxquant: Quantized neural networks via proximal operators. In *International Conference on Learning Representations*, 2019.
- Burak Bartan and Mert Pilanci. Neural spectrahedra and semidefinite lifts: Global convex optimization of polynomial activation neural networks in fully polynomial-time. *arXiv preprint arXiv:2101.02429*, 2021.
- Mohamed Ali Belabbas. On implicit regularization: Morse functions and applications to matrix factorization. *arXiv preprint arXiv:2001.04264*, 2020.
- Srinadh Bhojanapalli, Anastasios Kyriillidis, and Sujay Sanghavi. Dropping convexity for faster semi-definite optimization. In *Conference on Learning Theory*, pp. 530–582. PMLR, 2016.
- Davis Blalock, Jose Javier Gonzalez Ortiz, Jonathan Frankle, and John Guttag. What is the state of neural network pruning? *Proceedings of machine learning and systems*, 2:129–146, 2020.
- Nicolas Boumal, Vlad Voroninski, and Afonso Bandeira. The non-convex Burer-Monteiro approach works on smooth semidefinite programs. *Advances in Neural Information Processing Systems*, 29, 2016.
- Nicolas Boumal, Vladislav Voroninski, and Afonso S Bandeira. Deterministic guarantees for Burer-Monteiro factorizations of smooth semidefinite programs. *Communications on Pure and Applied Mathematics*, 73(3):581–608, 2020.
- Samuel Burer and Renato DC Monteiro. A nonlinear programming algorithm for solving semidefinite programs via low-rank factorization. *Mathematical programming*, 95(2):329–357, 2003.
- Samuel Burer and Renato DC Monteiro. Local minima and convergence in low-rank semidefinite programming. *Mathematical programming*, 103(3):427–444, 2005.
- Emmanuel Candes and Benjamin Recht. Exact matrix completion via convex optimization. *Communications of the ACM*, 55(6):111–119, 2012.

- Emmanuel J Candes, Thomas Strohmer, and Vladislav Voroninski. Phaselift: Exact and stable signal recovery from magnitude measurements via convex programming. *Communications on Pure and Applied Mathematics*, 66(8):1241–1274, 2013.
- Xiangyu Chang, Yingcong Li, Samet Oymak, and Christos Thrampoulidis. Provable benefits of overparameterization in model compression: From double descent to pruning neural networks. In *Proceedings of the AAAI Conference on Artificial Intelligence*, volume 35, pp. 6974–6983, 2021.
- Hongrong Cheng, Miao Zhang, and Javen Qinfeng Shi. A survey on deep neural network pruning: Taxonomy, comparison, analysis, and recommendations. *IEEE Transactions on Pattern Analysis and Machine Intelligence*, 2024.
- Diego Cifuentes. On the burer–monteiro method for general semidefinite programs. *Optimization Letters*, 15(6):2299–2309, 2021.
- Jia Deng, Wei Dong, Richard Socher, Li-Jia Li, Kai Li, and Li Fei-Fei. ImageNet: A large-scale hierarchical image database. In *2009 IEEE Conference on Computer Vision and Pattern Recognition*, pp. 248–255, 2009. doi: 10.1109/CVPR.2009.5206848.
- Timothy Dozat. Incorporating Nesterov momentum into Adam. 2016.
- Ebrahim Elgazar. Pixel art, 2024. URL <https://www.kaggle.com/datasets/ebrahimelgazar/pixel-art/>.
- Tolga Ergen and Mert Pilanci. Implicit convex regularizers of CNN architectures: Convex optimization of two-and three-layer networks in polynomial time. In *International Conference on Learning Representations*, 2020.
- Ruili Feng, Kecheng Zheng, Yukun Huang, Deli Zhao, Michael Jordan, and Zheng-Jun Zha. Rank diminishing in deep neural networks. *Advances in Neural Information Processing Systems*, 35: 33054–33065, 2022.
- Jonathan Fiat, Eran Malach, and Shai Shalev-Shwartz. Decoupling gating from linearity. *arXiv preprint arXiv:1906.05032*, 2019.
- Gauthier Gidel, Francis Bach, and Simon Lacoste-Julien. Implicit regularization of discrete gradient dynamics in linear neural networks. *Advances in Neural Information Processing Systems*, 32, 2019.
- Donald Goldfarb and Shiqian Ma. Convergence of fixed-point continuation algorithms for matrix rank minimization. *Foundations of Computational Mathematics*, 11(2):183–210, 2011.
- Ian Goodfellow, Yoshua Bengio, and Aaron Courville. *Deep Learning*. MIT Press, 2016.
- Jianping Gou, Baosheng Yu, Stephen J Maybank, and Dacheng Tao. Knowledge distillation: A survey. *International Journal of Computer Vision*, 129(6):1789–1819, 2021.
- Suriya Gunasekar, Blake E Woodworth, Srinadh Bhojanapalli, Behnam Neyshabur, and Nati Srebro. Implicit regularization in matrix factorization. *Advances in neural information processing systems*, 30, 2017.
- Tom Gunter, Zirui Wang, Chong Wang, Ruoming Pang, Andy Narayanan, Aonan Zhang, Bowen Zhang, Chen Chen, Chung-Cheng Chiu, David Qiu, et al. Apple Intelligence foundation language models. *arXiv preprint arXiv:2407.21075*, 2024.
- Song Han, Jeff Pool, John Tran, and William Dally. Learning both weights and connections for efficient neural network. *Advances in neural information processing systems*, 28, 2015.
- Babak Hassibi and David Stork. Second order derivatives for network pruning: Optimal brain surgeon. *Advances in neural information processing systems*, 5, 1992.

- Ya-Ping Hsieh, Yu-Chun Kao, Rabeeh Karimi Mahabadi, Alp Yurtsever, Anastasios Kyrillidis, and Volkan Cevher. A non-Euclidean gradient descent framework for non-convex matrix factorization. *IEEE Transactions on Signal Processing*, 66(22):5917–5926, 2018.
- Guang-Bin Huang. Learning capability and storage capacity of two-hidden-layer feedforward networks. *IEEE transactions on neural networks*, 14(2):274–281, 2003.
- Max Jaderberg, Andrea Vedaldi, and Andrew Zisserman. Speeding up convolutional neural networks with low rank expansions. *arXiv preprint arXiv:1405.3866*, 2014.
- Prateek Jain, Raghu Meka, and Inderjit Dhillon. Guaranteed rank minimization via singular value projection. *Advances in Neural Information Processing Systems*, 23, 2010.
- Steven A Janowsky. Pruning versus clipping in neural networks. *Physical Review A*, 39(12):6600, 1989.
- Zhipeng Jia, Xingyi Huang, I Eric, Chao Chang, and Yan Xu. Constrained deep weak supervision for histopathology image segmentation. *IEEE transactions on medical imaging*, 36(11):2376–2388, 2017.
- Hoel Kervadec, Jose Dolz, Meng Tang, Eric Granger, Yuri Boykov, and Ismail Ben Ayed. Constrained-CNN losses for weakly supervised segmentation. *Medical image analysis*, 54:88–99, 2019.
- Diederik P Kingma and Jimmy Ba. Adam: A method for stochastic optimization. *arXiv preprint arXiv:1412.6980*, 2014.
- Raghuraman Krishnamoorthi. Quantizing deep convolutional networks for efficient inference: A whitepaper. *arXiv preprint arXiv:1806.08342*, 2018.
- Anastasios Kyrillidis and Volkan Cevher. Matrix recipes for hard thresholding methods. *Journal of mathematical imaging and vision*, 48:235–265, 2014.
- Thien Le and Stefanie Jegelka. Training invariances and the low-rank phenomenon: beyond linear networks. In *International Conference on Learning Representations*, 2022.
- Vadim Lebedev, Yaroslav Ganin, Maksim Rakhuba, Ivan Oseledets, and Victor Lempitsky. Speeding-up convolutional neural networks using fine-tuned CP-decomposition. In *International Conference on Learning Representations*, 2015.
- Yann LeCun, Bernhard Boser, John Denker, Donnie Henderson, Richard Howard, Wayne Hubbard, and Lawrence Jackel. Handwritten digit recognition with a back-propagation network. *Advances in neural information processing systems*, 2, 1989a.
- Yann LeCun, John Denker, and Sara Solla. Optimal brain damage. *Advances in neural information processing systems*, 2, 1989b.
- Yann LeCun, Léon Bottou, Genevieve B Orr, and Klaus-Robert Müller. Efficient backprop. In *Neural networks: Tricks of the trade*, pp. 9–50. Springer, 2002.
- Yann LeCun, Corinna Cortes, and Christopher J. Burges. MNIST handwritten digit database. <http://yann.lecun.com/exdb/mnist/>, 2010.
- Ching-pei Lee, Ling Liang, Tianyun Tang, and Kim-Chuan Toh. Accelerating nuclear-norm regularized low-rank matrix optimization through Burer-Monteiro decomposition. *arXiv preprint arXiv:2204.14067*, 2022.
- Jason D Lee, Max Simchowitz, Michael I Jordan, and Benjamin Recht. Gradient descent converges to minimizers. *arXiv preprint arXiv:1602.04915*, 2016.
- Namhoon Lee, Thalaisyasingam Ajanthan, and Philip HS Torr. SNIP: Single-shot network pruning based on connection sensitivity. *arXiv preprint arXiv:1810.02340*, 2018.

- Zhiyuan Li, Yuping Luo, and Kaifeng Lyu. Towards resolving the implicit bias of gradient descent for matrix factorization: Greedy low-rank learning. In *International Conference on Learning Representations*, 2021.
- Lu Lu, Raphael Pestourie, Wenjie Yao, Zhicheng Wang, Francesc Verdugo, and Steven G Johnson. Physics-informed neural networks with hard constraints for inverse design. *SIAM Journal on Scientific Computing*, 43(6):B1105–B1132, 2021.
- Jan Macdonald, Mathieu E Besançon, and Sebastian Pokutta. Interpretable neural networks with Frank-Wolfe: Sparse relevance maps and relevance orderings. In *International Conference on Machine Learning*, pp. 14699–14716. PMLR, 2022.
- Pablo Márquez-Neila, Mathieu Salzmann, and Pascal Fua. Imposing hard constraints on deep networks: Promises and limitations. *arXiv preprint arXiv:1706.02025*, 2017.
- Michael C Mozer and Paul Smolensky. Skeletonization: A technique for trimming the fat from a network via relevance assessment. *Advances in neural information processing systems*, 1, 1988.
- Behnam Neyshabur. Implicit regularization in deep learning. *arXiv preprint arXiv:1709.01953*, 2017.
- Behnam Neyshabur, Ryota Tomioka, and Nathan Srebro. In search of the real inductive bias: On the role of implicit regularization in deep learning. *arXiv preprint arXiv:1412.6614*, 2014.
- Behnam Neyshabur, Srinadh Bhojanapalli, David McAllester, and Nati Srebro. Exploring generalization in deep learning. *Advances in neural information processing systems*, 30, 2017.
- Dohyung Park, Anastasios Kyrillidis, Constantine Carmanis, and Sujay Sanghavi. Non-square matrix sensing without spurious local minima via the Burer-Monteiro approach. In *Artificial Intelligence and Statistics*, pp. 65–74. PMLR, 2017.
- Dohyung Park, Anastasios Kyrillidis, Constantine Caramanis, and Sujay Sanghavi. Finding low-rank solutions via nonconvex matrix factorization, efficiently and provably. *SIAM Journal on Imaging Sciences*, 11(4):2165–2204, 2018.
- Rahul S Patel, Sharad Bhartiya, and Ravindra D Gudi. Physics constrained learning in neural network based modeling. *IFAC-PapersOnLine*, 55(7):79–85, 2022.
- Deepak Pathak, Philipp Krahenbuhl, and Trevor Darrell. Constrained convolutional neural networks for weakly supervised segmentation. In *Proceedings of the IEEE international conference on computer vision*, pp. 1796–1804, 2015.
- Mert Pilanci and Tolga Ergen. Neural networks are convex regularizers: Exact polynomial-time convex optimization formulations for two-layer networks. In *International Conference on Machine Learning*, pp. 7695–7705. PMLR, 2020.
- Sebastian Pokutta, Christoph Spiegel, and Max Zimmer. Deep neural network training with Frank-Wolfe. *arXiv preprint arXiv:2010.07243*, 2020.
- Karthik Prakhya, Tolga Birdal, and Alp Yurtsever. Convex formulations for training two-layer ReLU neural networks. *arXiv preprint arXiv:2410.22311*, 2024.
- Ilija Radosavovic, Raj Prateek Kosaraju, Ross Girshick, Kaiming He, and Piotr Dollár. Designing network design spaces, 2020.
- Maziar Raissi, Paris Perdikaris, and George E Karniadakis. Physics-informed neural networks: A deep learning framework for solving forward and inverse problems involving nonlinear partial differential equations. *Journal of Computational physics*, 378:686–707, 2019.
- Noam Razin and Nadav Cohen. Implicit regularization in deep learning may not be explainable by norms. *Advances in neural information processing systems*, 33:21174–21187, 2020.

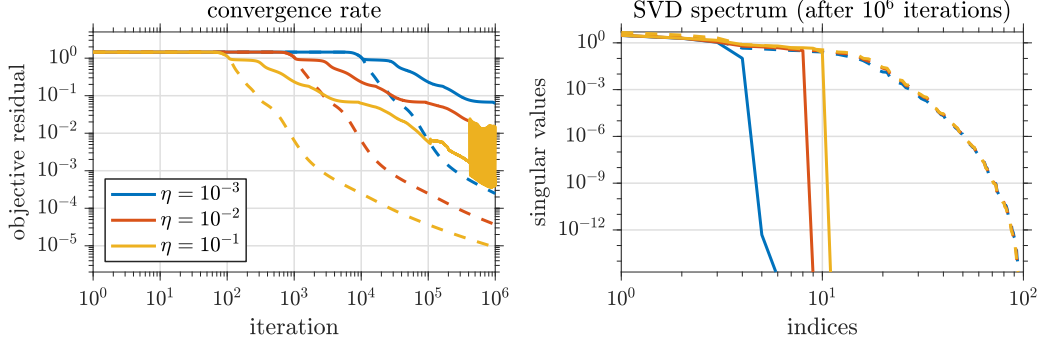
- Benjamin Recht, Maryam Fazel, and Pablo A Parrilo. Guaranteed minimum-rank solutions of linear matrix equations via nuclear norm minimization. *SIAM review*, 52(3):471–501, 2010.
- Russell Reed. Pruning algorithms—a survey. *IEEE transactions on Neural Networks*, 4(5):740–747, 1993.
- Meg Risdal. New York City taxi trip duration, 2017. URL <https://kaggle.com/competitions/ny-c-taxi-trip-duration>.
- Mehmet Fatih Sahin, Ahmet Alacaoglu, Fabian Latorre, Volkan Cevher, et al. An inexact augmented Lagrangian framework for nonconvex optimization with nonlinear constraints. *Advances in Neural Information Processing Systems*, 32, 2019.
- Arda Sahiner, Tolga Ergen, John M Pauly, and Mert Pilanci. Vector-output ReLU neural network problems are copositive programs: Convex analysis of two layer networks and polynomial-time algorithms. In *International Conference on Learning Representations*, 2021.
- Arda Sahiner, Tolga Ergen, Batu Ozturkler, John M Pauly, Morteza Mardani, and Mert Pilanci. Scaling convex neural networks with Burer-Monteiro factorization. In *The Twelfth International Conference on Learning Representations*, 2023.
- Tara N Sainath, Brian Kingsbury, Vikas Sindhvani, Ebru Arisoy, and Bhuvana Ramabhadran. Low-rank matrix factorization for deep neural network training with high-dimensional output targets. In *2013 IEEE international conference on acoustics, speech and signal processing*, pp. 6655–6659. IEEE, 2013.
- Simone Scardapane, Danilo Comminiello, Amir Hussain, and Aurelio Uncini. Group sparse regularization for deep neural networks. *Neurocomputing*, 241:81–89, 2017.
- Ruoyu Sun and Zhi-Quan Luo. Guaranteed matrix completion via non-convex factorization. *IEEE Transactions on Information Theory*, 62(11):6535–6579, 2016.
- Ilya Sutskever, James Martens, George Dahl, and Geoffrey Hinton. On the importance of initialization and momentum in deep learning. In *International conference on machine learning*, pp. 1139–1147. PMLR, 2013.
- Sridhar Swaminathan, Deepak Garg, Rajkumar Kannan, and Frederic Andres. Sparse low rank factorization for deep neural network compression. *Neurocomputing*, 398:185–196, 2020.
- Mingxing Tan and Quoc Le. Efficientnet: Rethinking model scaling for convolutional neural networks. In *International conference on machine learning*, pp. 6105–6114. PMLR, 2019.
- Nadav Timor, Gal Vardi, and Ohad Shamir. Implicit regularization towards rank minimization in ReLU networks. In *International Conference on Algorithmic Learning Theory*, pp. 1429–1459. PMLR, 2023.
- Zhengzhong Tu, Hossein Talebi, Han Zhang, Feng Yang, Peyman Milanfar, Alan Bovik, and Yinxiao Li. MaxViT: Multi-axis vision transformer. In *European conference on computer vision*, pp. 459–479. Springer, 2022.
- Ashish Vaswani, Noam Shazeer, Niki Parmar, Jakob Uszkoreit, Llion Jones, Aidan N Gomez, Łukasz Kaiser, and Illia Polosukhin. Attention is all you need. *Advances in neural information processing systems*, 30, 2017.
- Irene Waldspurger and Alden Waters. Rank optimality for the burer–monteiro factorization. *SIAM journal on Optimization*, 30(3):2577–2602, 2020.
- Patrick Weber, Jeremy Geiger, and Werner Wagner. Constrained neural network training and its application to hyperelastic material modeling. *Computational Mechanics*, 68:1179–1204, 2021.

- Jian Xue, Jinyu Li, and Yifan Gong. Restructuring of deep neural network acoustic models with singular value decomposition. In *Interspeech*, pp. 2365–2369, 2013.
- Baturalp Yalçın, Ziyi Ma, Javad Lavaei, and Somayeh Sojoudi. Semidefinite programming versus burer-monteiro factorization for matrix sensing. In *Proceedings of the AAAI Conference on Artificial Intelligence*, volume 37, pp. 10702–10710, 2023.
- Liu Yang, Jifan Zhang, Joseph Shenouda, Dimitris Papailiopoulos, Kangwook Lee, and Robert D Nowak. PathProx: A proximal gradient algorithm for weight decay regularized deep neural networks. *arXiv preprint arXiv:2210.03069*, 2022.
- Yang Yang, Yaxiong Yuan, Avraam Chatzimichailidis, Ruud JG van Sloun, Lei Lei, and Symeon Chatzinotas. ProxSGD: Training structured neural networks under regularization and constraints. In *International Conference on Learning Representations*, 2020.
- Jihun Yun, Aurélie C Lozano, and Eunho Yang. Adaptive proximal gradient methods for structured neural networks. *Advances in Neural Information Processing Systems*, 34:24365–24378, 2021.
- Alp Yurtsever, Alex Gu, and Suvrit Sra. Three operator splitting with subgradients, stochastic gradients, and adaptive learning rates. *Advances in Neural Information Processing Systems*, 34: 19743–19756, 2021.
- Max Zimmer, Christoph Spiegel, and Sebastian Pokutta. Compression-aware training of neural networks using Frank-Wolfe. *arXiv preprint arXiv:2205.11921*, 2022.

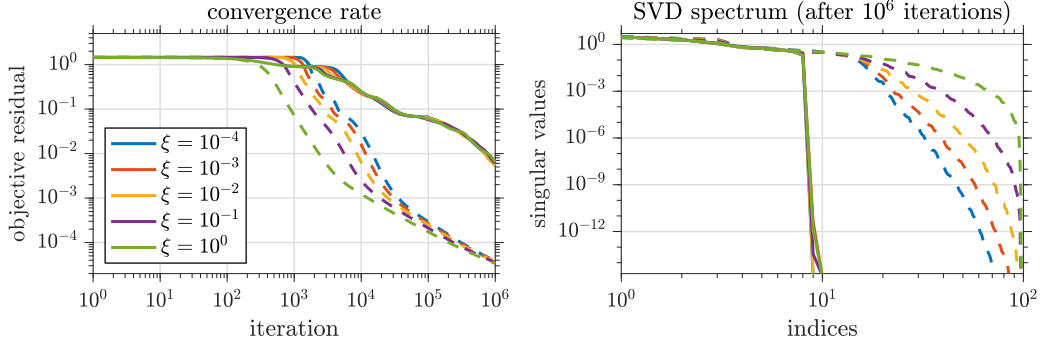
A Additional Details on Matrix Factorization Experiments

A.1 Matrix Completion under Gaussian Noise

We conducted similar experiments to those in Section 3.2 also using noisy measurements: Let $b^\natural = \mathcal{A}(X^\natural)$ represent the true measurements, and assume $b = b^\natural + \omega$, where $\omega \in \mathbb{R}^n$ is zero-mean Gaussian noise with a standard deviation of $\sigma = 10^{-2}\|b\|_2$. The results, shown in Figure SM1, remain consistent with the noiseless case. UDU^\top exhibits implicit bias toward truly low-rank solutions, while the classical BM factorization yields approximately low-rank solutions, with the spectral decay influenced by initialization.



Impact of **step-size** (η), under **Gaussian noise**, with fixed initialization.



Impact of **initial distance to origin** (ξ), under **Gaussian noise**, with fixed step-size.

Figure SM1: Impact of step-size and initialization on implicit bias. **Solid lines represent our UDU factorization**, while **dashed lines denote the classical BM factorization**. [Left] Objective residual vs. iterations. [Right] Singular value spectrum after 10^6 iterations.

A.2 UDU Factorization Produces Rank-Revealing Solutions

The proposed factorization method naturally produces rank-revealing solutions. The columns of U converge to zero in certain directions, resulting in truly low-rank solutions. Specifically, U tends to grow along specific directions while the rescaling induced by projection onto the bounded constraint shrinks other coordinates. This behavior resembles the mechanism of the power method and provides insights into its connection with divergent forces.

In Figure SM2, we illustrate the evolution of the column norms of U from the matrix completion experiment described in Section 3.2. Figure SM3 displays the corresponding entries in the diagonal factor D . For comparison, Figure SM4 shows the column norms of U obtained from the same experiment using the standard BM factorization. The results are shown for $\xi = 10^{-1}$ and $\eta = 10^{-1}$ over 10^5 iterations, but the findings are similar across other parameter settings. We also repeat the experiment with the noisy measurements described in Appendix A.1. The results are shown in Figures SM5 to SM7.

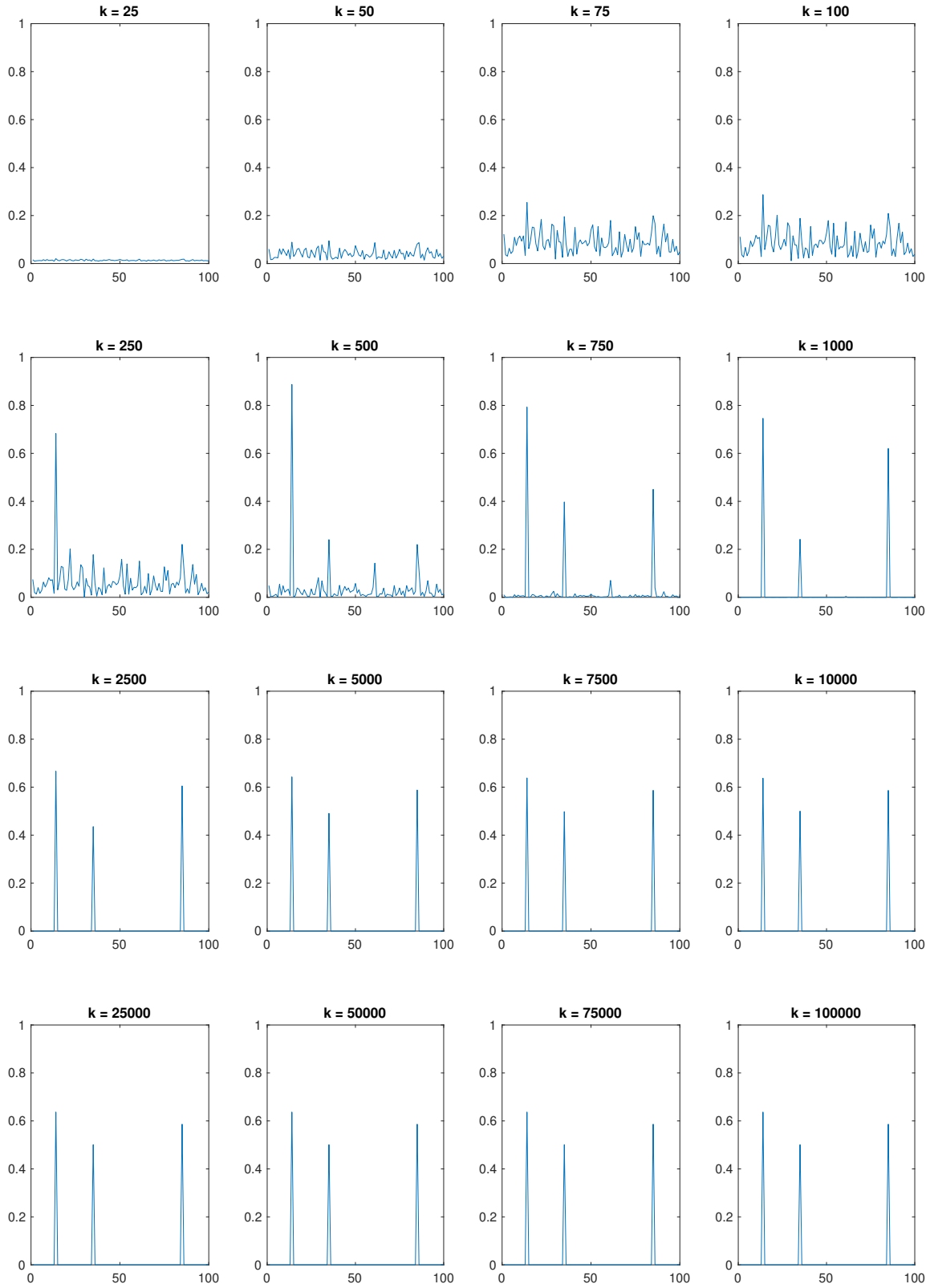


Figure SM2: Evolution of the column norms of U during the matrix completion experiment using the UDU factorization. The x-axis represents column indices, and the y-axis shows the Euclidean norms of the columns.

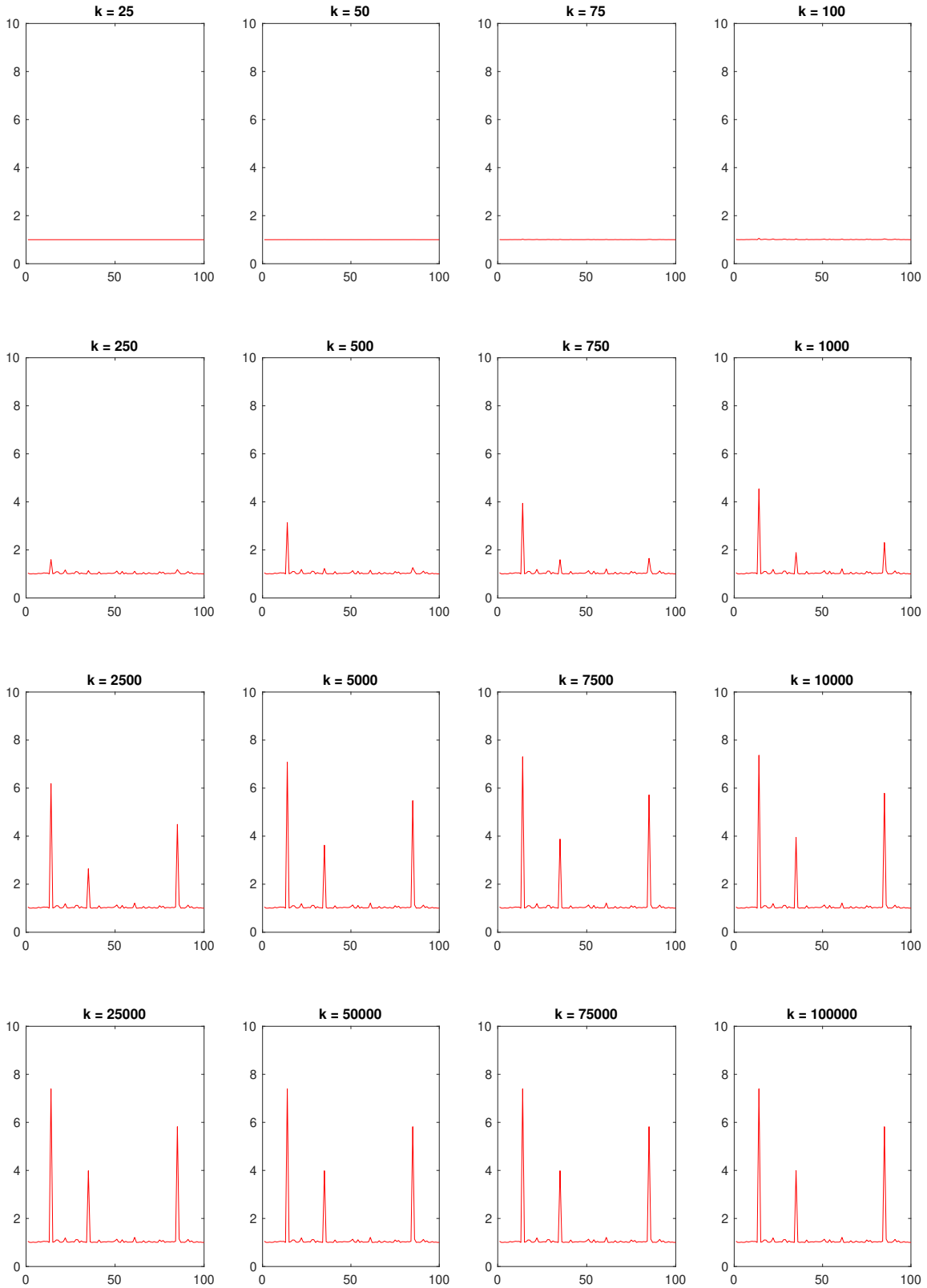


Figure SM3: Evolution of the diagonal entries of D during the matrix completion experiment using the UDU factorization. The x-axis represents indices.

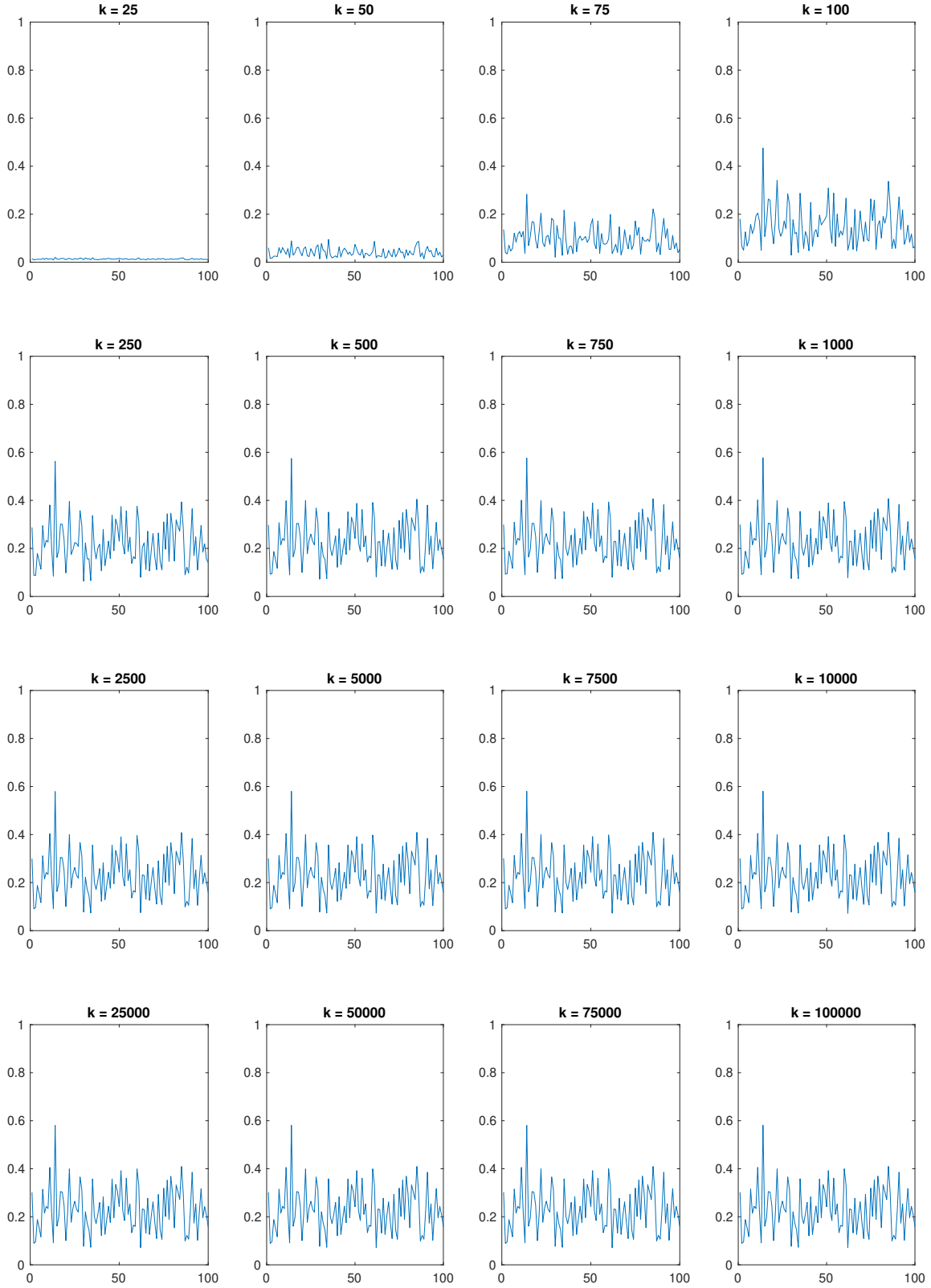


Figure SM4: Evolution of the column norms of U during the matrix completion experiment using the standard BM factorization, shown for comparison. The x-axis represents column indices, and the y-axis shows the Euclidean norms of the columns.

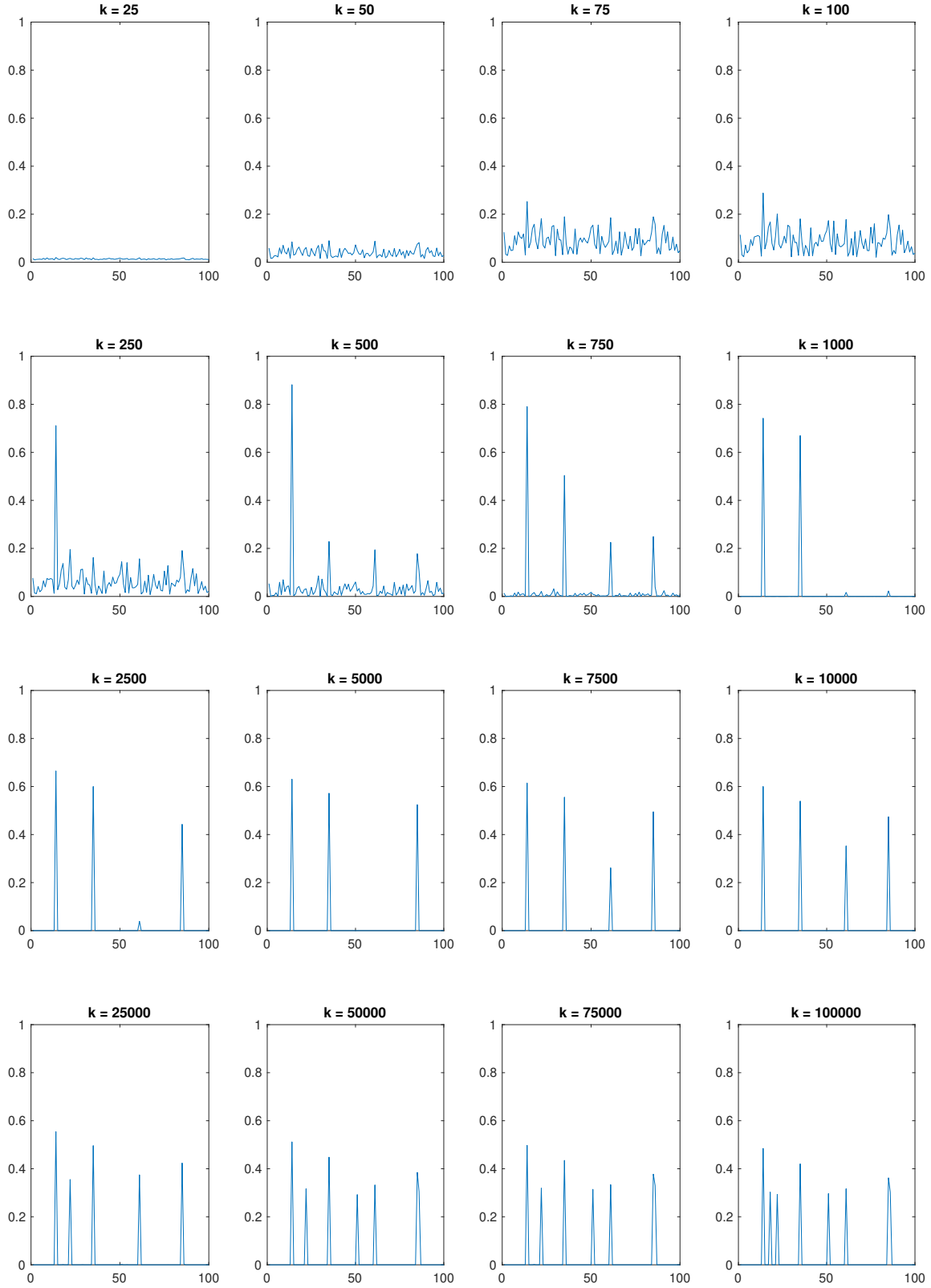


Figure SM5: Evolution of the column norms of U during the matrix completion experiment using the UDU factorization with **noisy** measurements. The x-axis represents column indices, and the y-axis shows the Euclidean norms of the columns.

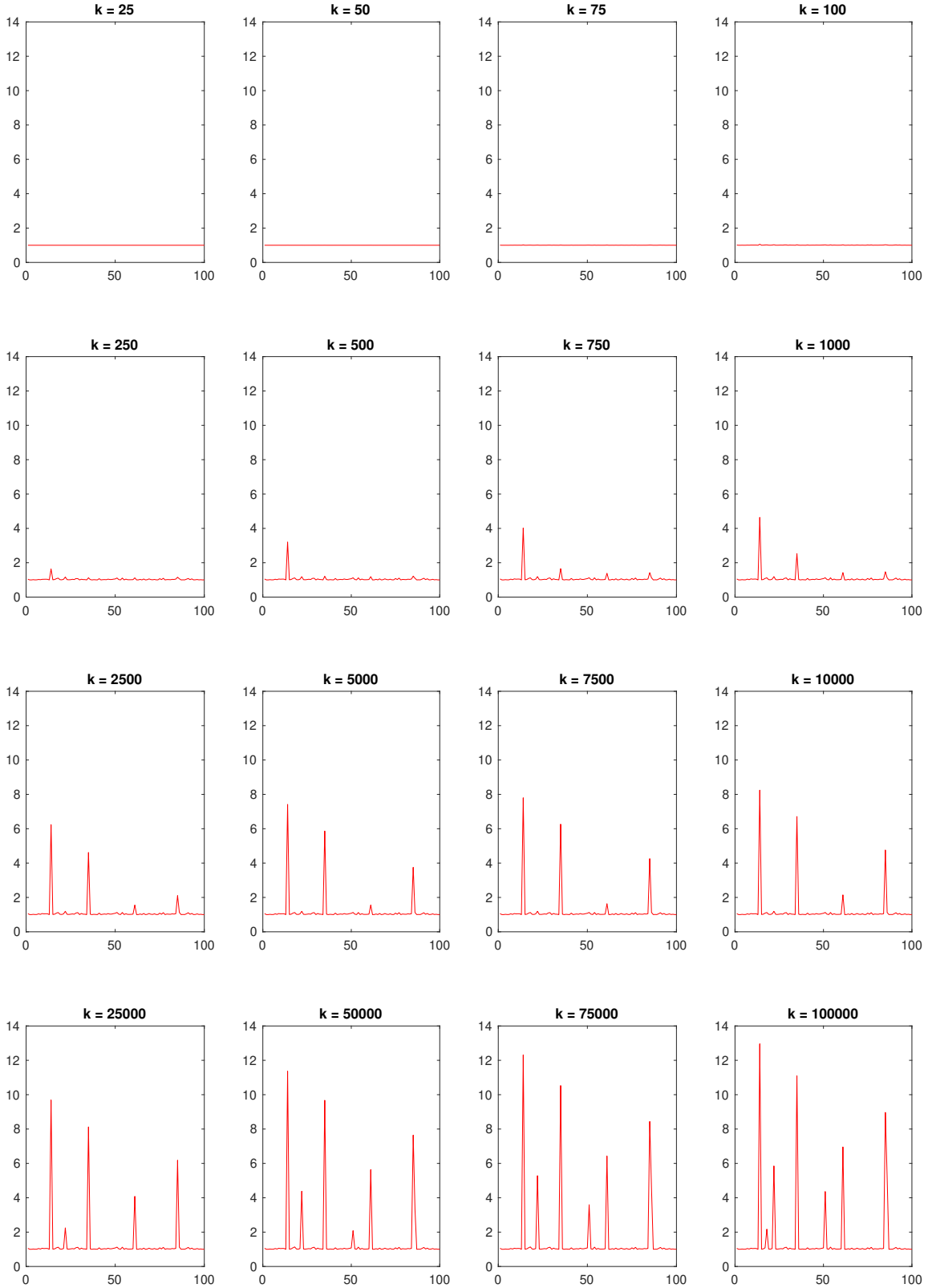


Figure SM6: Evolution of the diagonal entries of D during the matrix completion experiment using the UDU factorization with **noisy** measurements. The x-axis represents indices.

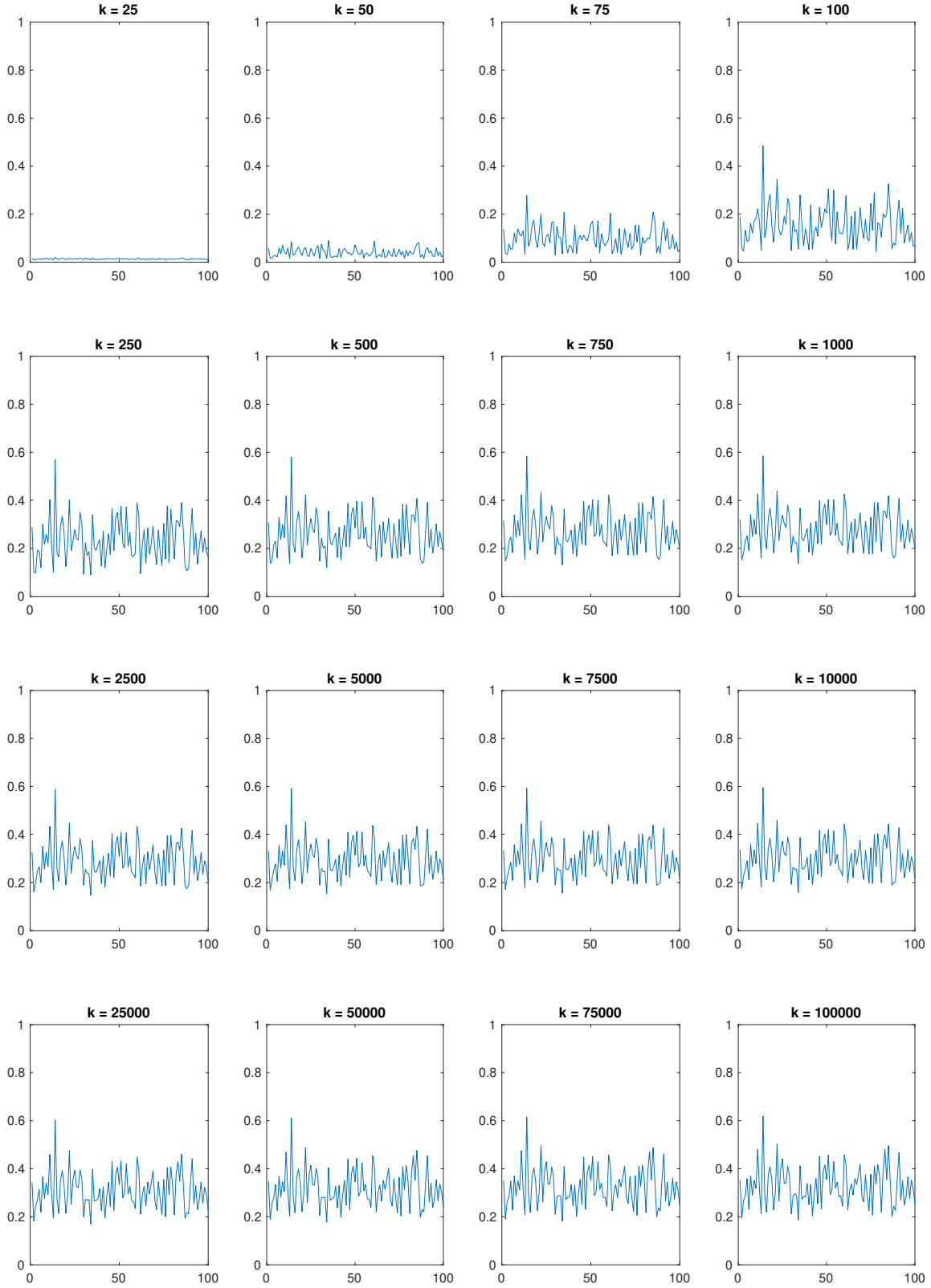


Figure SM7: Evolution of the column norms of U during the matrix completion experiment using the standard BM factorization with **noisy** measurements, shown for comparison. The x-axis represents column indices, and the y-axis shows the Euclidean norms of the columns.

A.3 Phase Retrieval Image Recovery

We conduct a numerical experiment on the matrix sensing problem arising in phase retrieval image recovery (Candes et al., 2013). The objective is to recover a signal from its quadratic measurements of the form $y_i = |\langle a_i, x \rangle|^2$. Although the standard maximum likelihood estimators lead to a non-convex optimization problem due to the quadratic terms, the problem can be reformulated as minimizing a convex function under a rank constraint in a lifted space. By denoting the lifted variable as $X = xx^\top$, the measurements can be expressed as

$$y_i = \langle a_i^\top x, a_i^\top x \rangle = \langle a_i a_i^\top, xx^\top \rangle := \langle A_i, X \rangle,$$

which allows us to reformulate the problem as

$$\min_{X \in \mathbb{S}_+^{d \times d}} \frac{1}{2} \|\mathcal{A}(X) - b\|_2^2 \quad \text{subj. to} \quad \text{rank}(X) \leq 1,$$

representing a special case of problem (1).

In this experiment, we use a gray-scale image of size 16×16 pixels, selected from the Pixel Art dataset (Elgazar, 2024), as the signal $x \in \mathbb{R}^n$ to recover, where $n = 256$. We generate a synthetic measurement system by sampling a_1, \dots, a_m from the standard Gaussian distribution, with $m = 2n$. We then solve problems (2) and (4). We initialized $U_0 \in \mathbb{R}^{n \times n}$ with entries drawn *iid* from the standard Gaussian distribution, then rescaled to have a unit Frobenius norm. For $D_0 \in \mathbb{R}^{n \times n}$, we used the identity matrix. We used step-size $\eta = \frac{1}{L}$ where L denotes the smoothness constant. After solving the problem, we recover $x \in \mathbb{R}^n$ from the lifted variable $X \in \mathbb{R}^{n \times n}$ by selecting its dominant eigenvector.

Figure SM8 demonstrates that the proposed method consistently identifies low-rank solutions, in line with the results of our other experiments. Figure SM9 displays the recovered image, demonstrating that the proposed method achieves higher quality than BM factorization within the same number of iterations, which can be attributed to the low-rank structure of the solution.

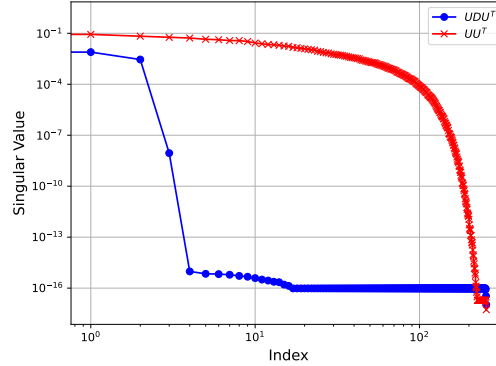


Figure SM8: Comparison of singular value spectrum in recovered image between methods based on UDU^T and UU^T .

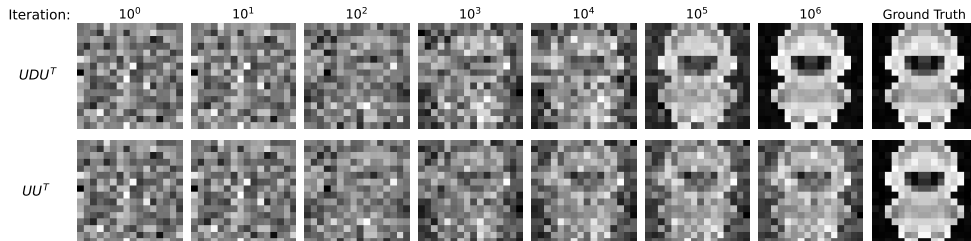


Figure SM9: Comparison of recovered image between methods based on UDU^T and UU^T .

B Additional Details on Neural Network Experiments

B.1 Design Variants of the UDV Architecture

When designing our network architecture, we considered four variants, including the one presented in [Section 4](#). The three additional models were defined by the following sets of constraints:

$$\sum_{j=1}^m \|\mathbf{u}_j\|_2^2 \leq 1, \quad \sum_{j=1}^m \|\mathbf{v}_j\|_2^2 \leq 1 \quad (\text{UDV-s})$$

$$\|\mathbf{u}_j\|_2^2 \leq 1, \quad \|\mathbf{v}_j\|_2^2 \leq 1 \quad w_j \geq 0; \quad \text{for all } j = 1, \dots, m \quad (\text{UDV-v1})$$

$$\|\mathbf{u}_j\|_2^2 \leq 1, \quad \|\mathbf{v}_j\|_2^2 \leq 1; \quad \text{for all } j = 1, \dots, m \quad (\text{UDV-v2})$$

In detail, UDV-s is identical to UDV but omits the non-negativity constraints on the diagonal layer. UDV-v1, on the other hand, enforces row/column-wise norm constraints instead of the Frobenius norm used in UDV, while retaining the non-negativity constraints on the diagonal elements. Finally, UDV-v2 is identical to UDV-v1 but without the non-negativity constraints on the diagonal layer.

We only report results from UDV, as defined in equation (7), in the main text. However, we provide results for the other variants in the Appendices for completeness and to illustrate the impact of different constraint settings on model performance.

[Figure SM11](#) and [Figure SM12](#) show that UDV consistently finds a low-rank solution. Generally, UDV exhibits the most pronounced decaying pattern in singular values. Additionally, we extended our experiments to include full-batch training on the HPART and NYCTTD datasets. Although full-batch training converges more slowly than stochastic (mini-batch) methods, it exhibits a similar singular value decay pattern, confirming our earlier observations.

B.2 Comparison of Model Performance with the MBGDM Algorithm

In [Section 4.1](#), we presented the performance of each model (UDV, UV, and UV-ReLU) in terms of generalization power (measured by validation loss or validation accuracy) along with the corresponding singular value spectrum, as shown in [Table 1](#) and [Figure 3](#). The results were obtained by selecting the optimal algorithm and learning rate pair for each model. Here, we conduct the same experiment, but focus exclusively on the MBGDM algorithm. The results, presented in [Table SM1](#) and [Figure SM10](#) are similar to the ones in [Section 4.1](#), showing similar trends, highlighting consistency across methods.

Table SM1: Model performance using MBGDM. M, E, and R represent the transferred models MaxVit-T, EfficientNet-B0, and RegNetX-32GF, respectively.

Tasks	Regression (Test Loss)		Classification (Test Accuracy)		
Dataset	HPART	NYCTTD	MNIST		
UDV	1.345×10^{-3}	5.248×10^{-6}	M: 99.67%	E: 99.63%	R: 99.74%
	MBGDM: 10^{-1}	MBGDM: 10^{-1}	MBGDM: 10^{-2}	MBGDM: 10^{-1}	MBGDM: 10^{-2}
UV	1.337×10^{-3}	5.259×10^{-6}	M: 99.69%	E: 99.59%	R: 99.56%
	MBGDM: 10^{-2}	MBGDM: 10^{-1}	MBGDM: 10^{-2}	MBGDM: 10^{-1}	MBGDM: 10^{-1}
UV-ReLU	1.244×10^{-3}	5.264×10^{-6}	M: 99.63%	E: 99.68%	R: 99.66%
	MBGDM: 10^{-1}	MBGDM: 10^{-1}	MBGDM: 10^{-2}	MBGDM: 10^{-1}	MBGDM: 10^{-1}

B.3 Additional Details on the Pruning Experiment

The SVD-based pruning experiments yield conclusions consistent with the singular value decay pattern. UDV typically exhibits the fastest decay, leading to more compact models while maintaining performance, as shown in [Figure SM13](#).

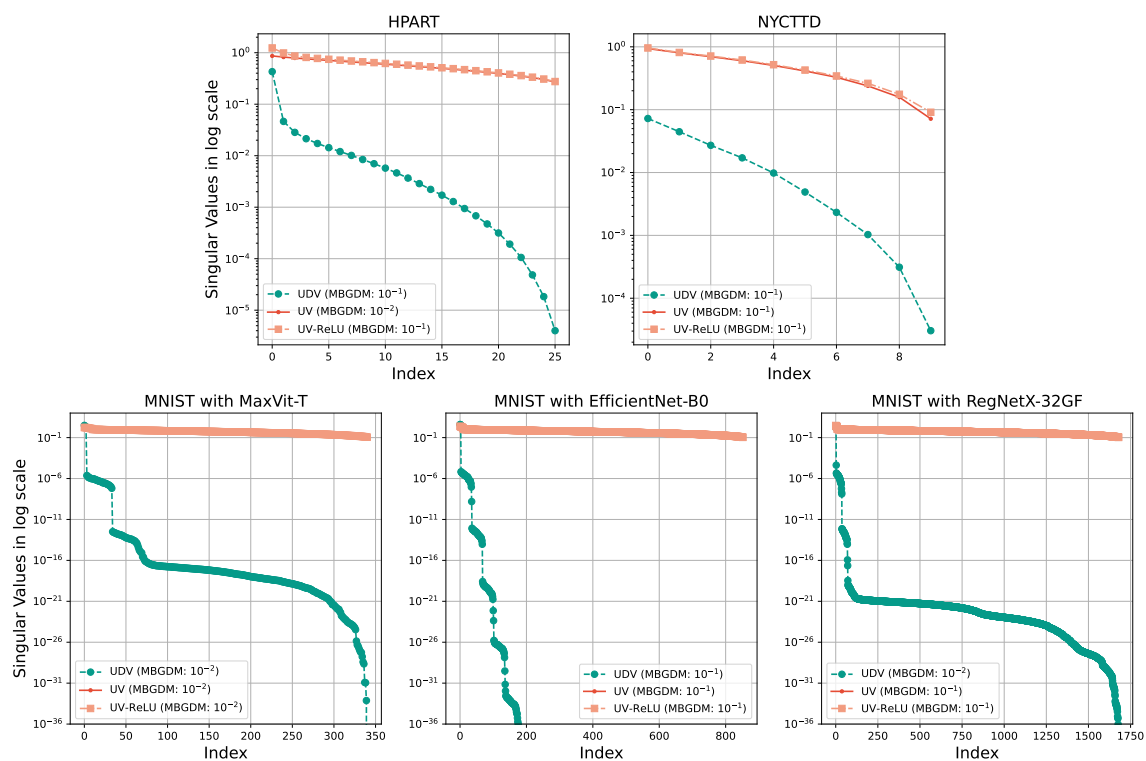


Figure SM10: Singular value spectrum corresponding to Table SM1.

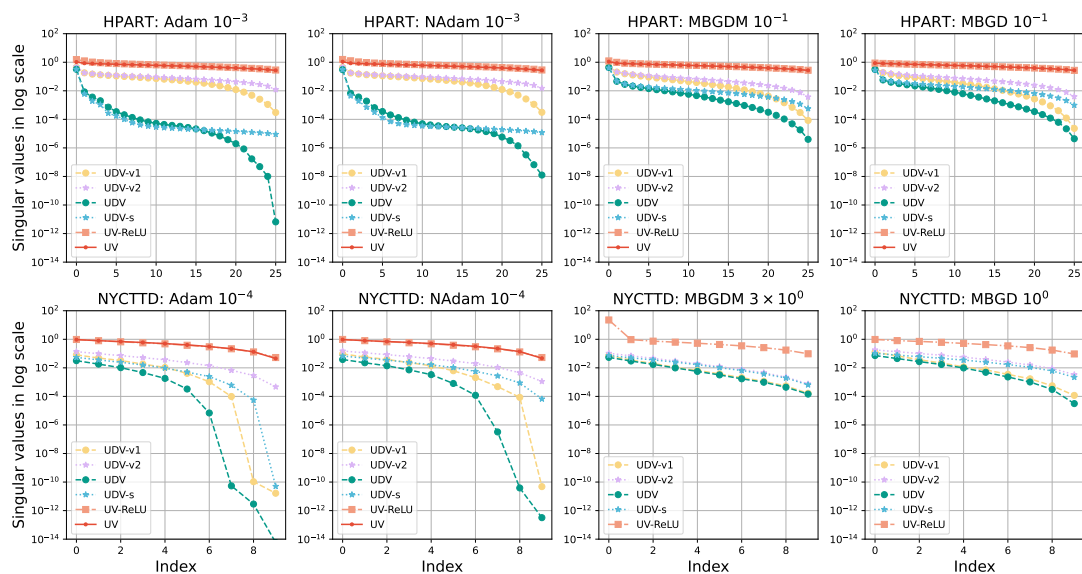


Figure SM11: Comparison of singular value pattern among all UDV variants, UV-ReLU and UV on the regression tasks.

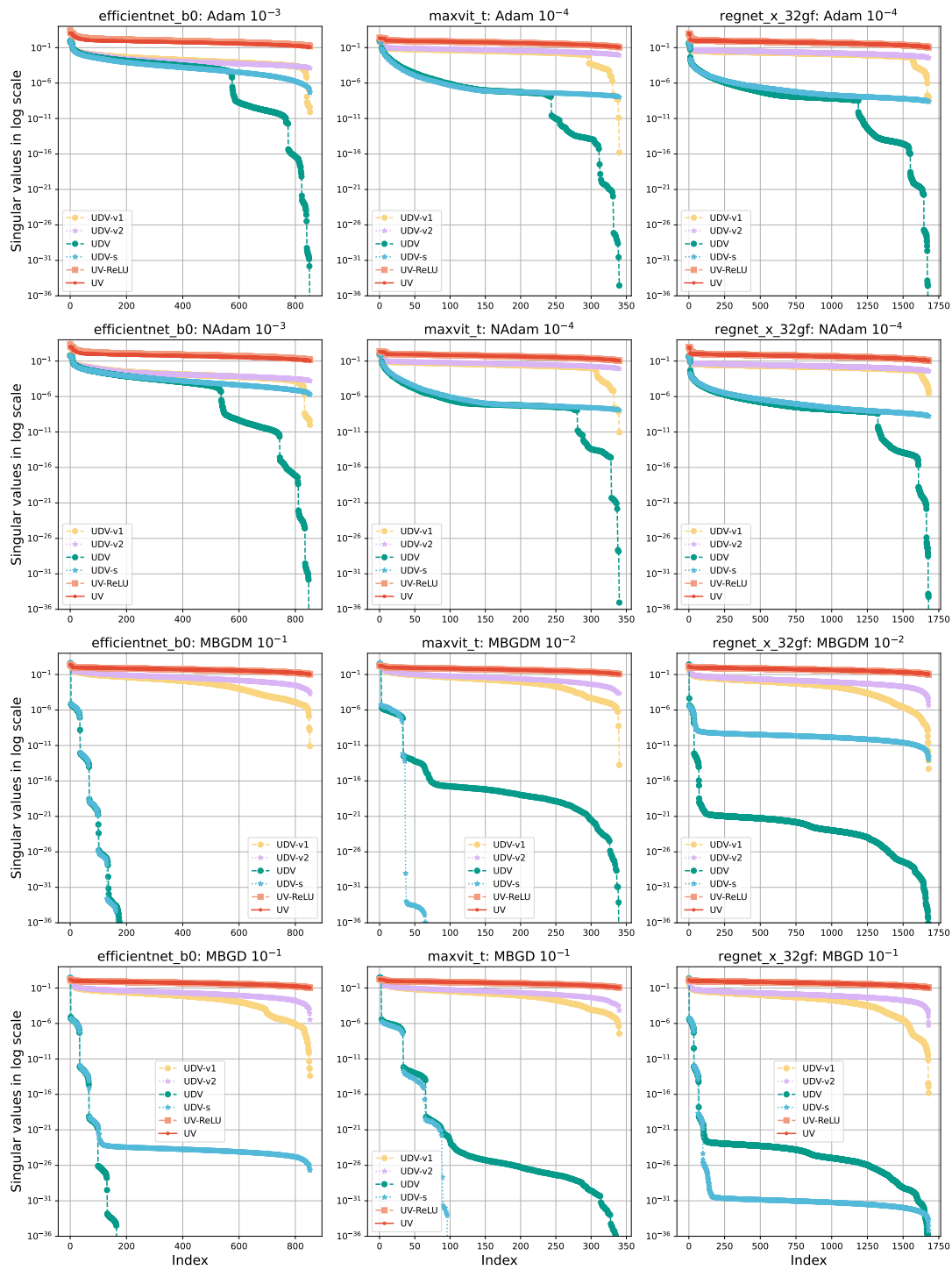


Figure SM12: Comparison of singular value pattern among all UDV variants, UV-ReLU and UV on the MNIST dataset.

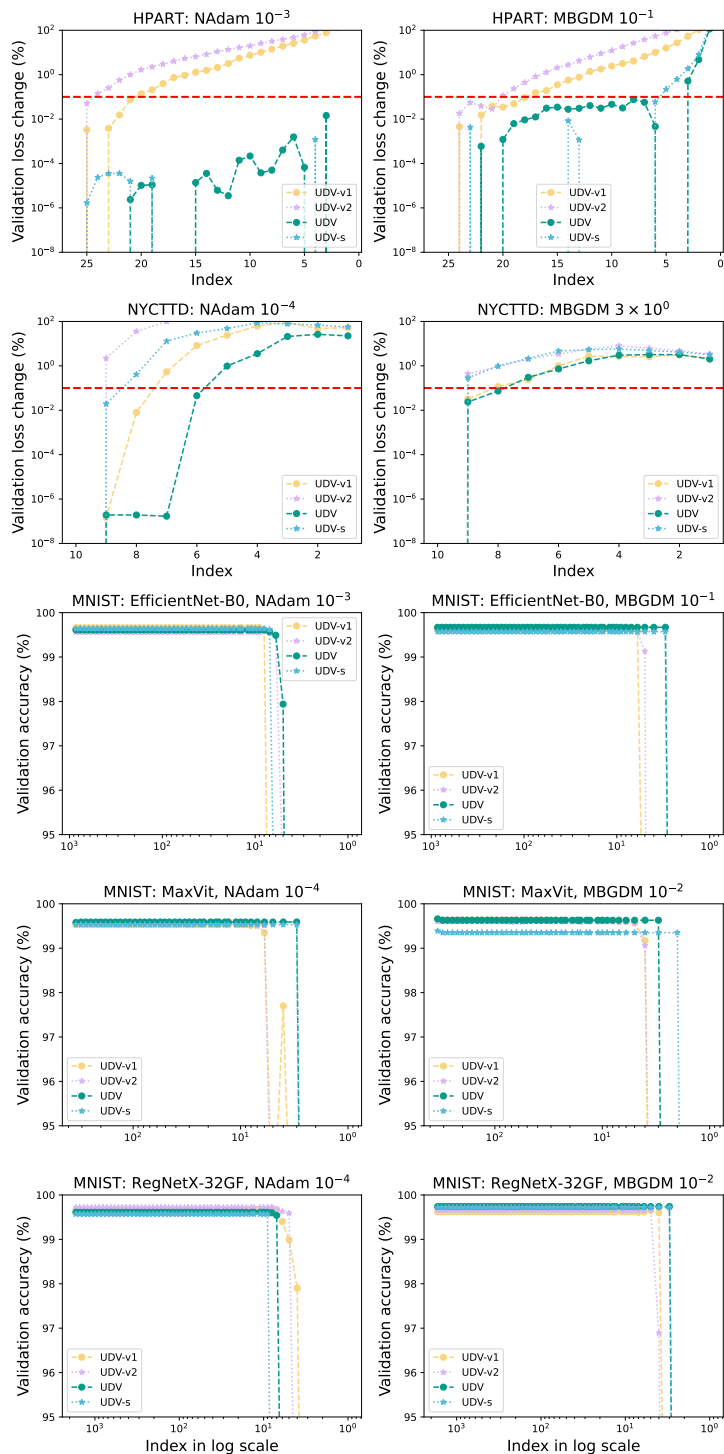


Figure SM13: The performance of SVD-based pruning. The index in x-axis represents the number of neurons in the diagonal layer after pruning. For the HPART and NYCTTD datasets, the validation loss change indicates how much worse the pruned model performs compared to the baseline (the model before pruning), expressed as a percentage ($\frac{\text{loss}_{\text{pruned}} - \text{loss}_{\text{baseline}}}{\text{loss}_{\text{baseline}}} \times 100\%$). Note that the pruned model may outperform the baseline, but negative values cannot be displayed on a logarithmic scale. The red dashed line denotes the 0.1% threshold, indicating negligible performance sacrifice. For the MNIST dataset, the results show the validation accuracy after pruning the model.

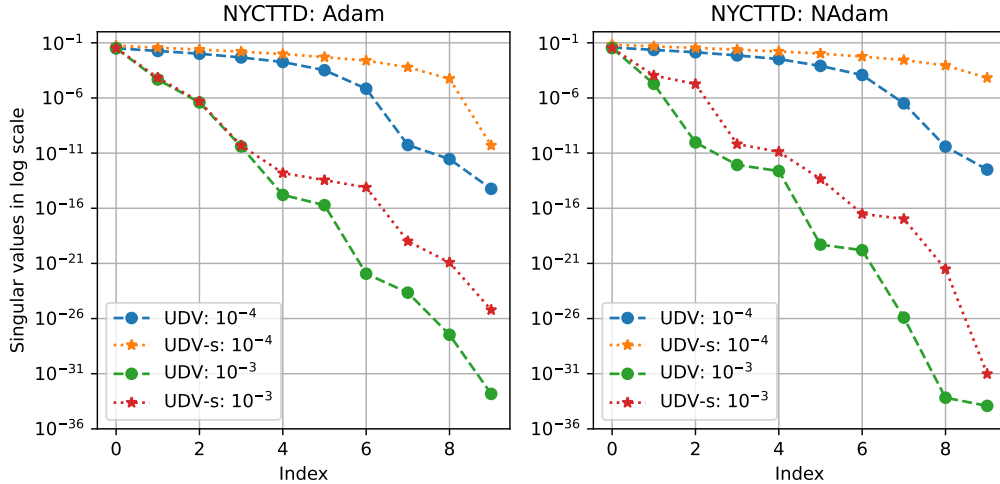


Figure SM14: Differences in singular value patterns across varying learning rates.

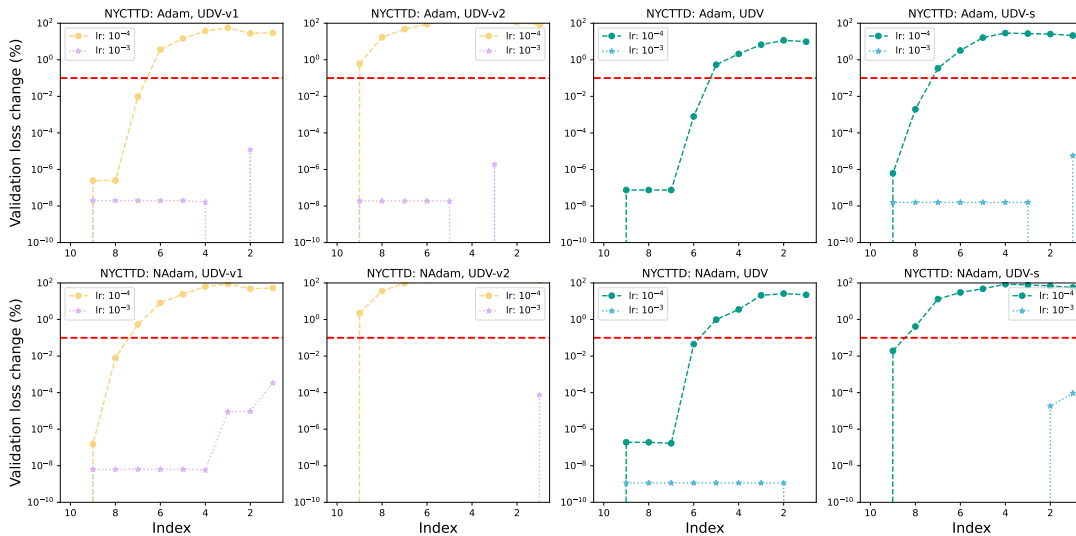


Figure SM15: Different learning rates lead different pruning performance. the validation loss change indicates how much worse the pruned model performs compared to the baseline (the model before pruning), expressed as a percentage ($\frac{loss_{pruned} - loss_{baseline}}{loss_{baseline}} \times 100\%$). Note that the pruned model may outperform the baseline, but negative values cannot be displayed on a logarithmic scale. The red dashed line denotes the 0.1% threshold, indicating negligible performance sacrifice.

We observed that the learning rate can have some impact on the singular value decay pattern. In particular, a very large learning rate may cause oscillations in both training and validation loss, yet may result in a rapid decay of the spectrum. Conversely, a small learning rate may lead to a less pronounced spectral decay but still can yield a comparable validation loss to that of the optimal learning rates. For example, the difference in validation losses between the Adam optimizer with learning rates of $1e-3$ and $1e-4$ was negligible, yet the singular value spectra differed (see Figure SM14). This discrepancy also affects the performance of the pruning experiments (see Figure SM15).

When the learning rate is close to the optimal value, a ‘stair-step’ pattern (see Figure SM16) can be observed on the loss or accuracy curve in the classification task. It could be attributed to the model continuously searching for a low-rank solution, increasing the rank gradually.

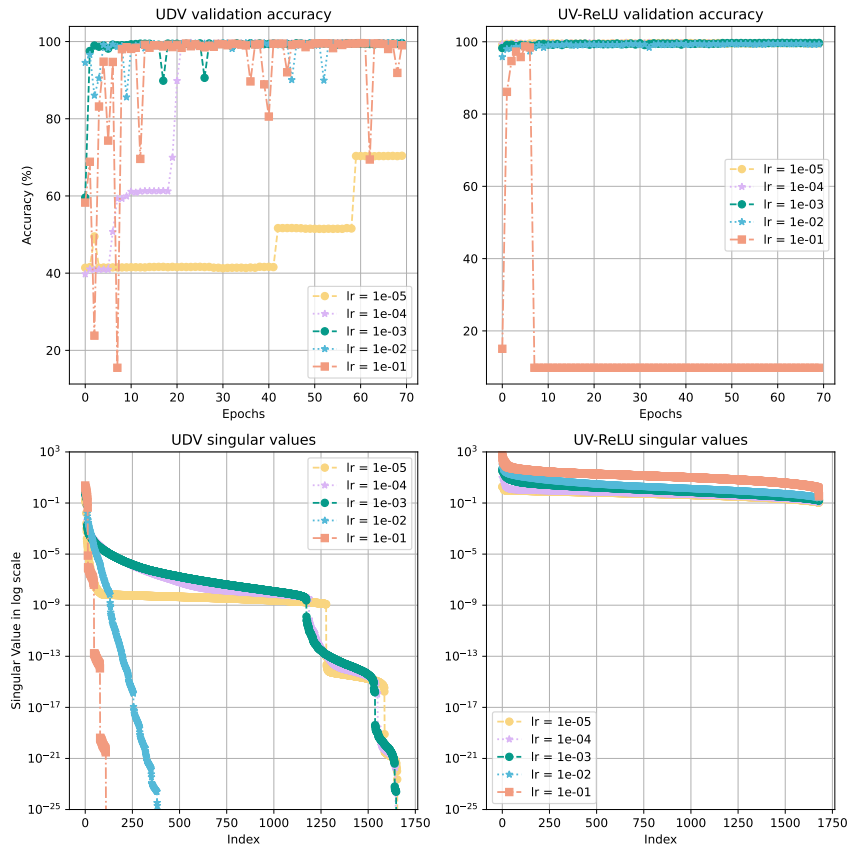


Figure SM16: The ‘stair-step’ accuracy curve in classification (RegNetX-32GF with Adam). The sub-figures in the second row correspond to the respective singular value spectra, indicating that UDV consistently seeks low-rank solutions regardless of the learning rate.

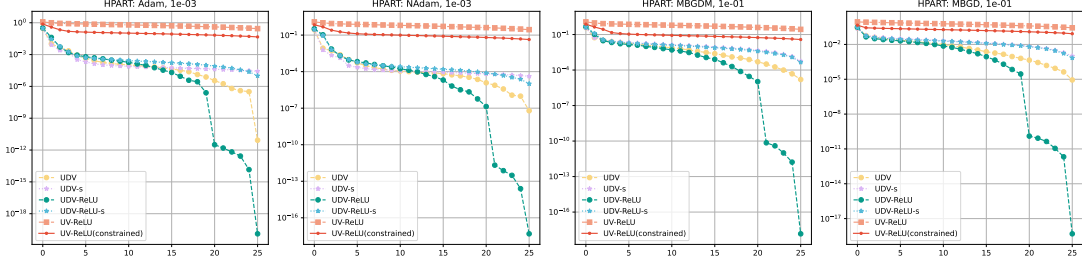


Figure SM17: ReLU in UDV: Singular value pattern on HPART dataset.

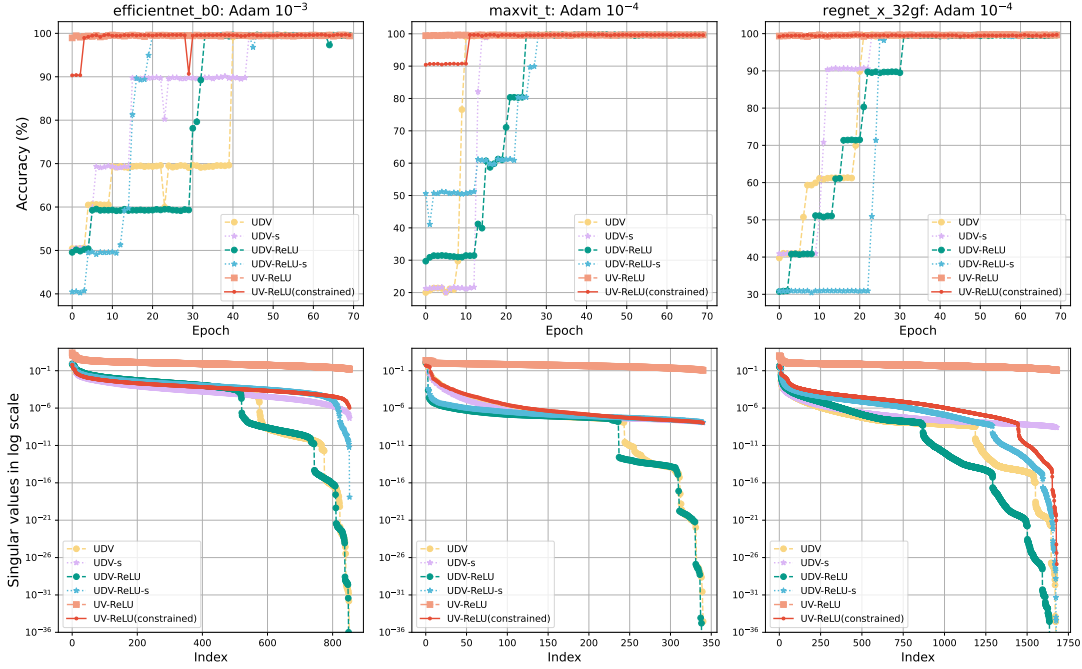


Figure SM18: ReLU in UDV: Validation accuracy (the first row) and the singular value pattern (the second row) on MNIST dataset. Faster convergence can be achieved by fine-tuning the learning rate.

B.4 Incorporating ReLU into UDV

To explore whether non-linear activation functions, particularly ReLU, can be used in our UDV framework, we conducted an additional experiment.

Building on the standard ReLU, we first introduced norm constraints, $\sum_{j=1}^m \|\mathbf{u}_j\|_2^2 \leq 1$ and $\sum_{j=1}^m \|\mathbf{v}_j\|_2^2 \leq 1$, to the layers both before and after ReLU, denoted as *ReLU(constrained)*. Next, we integrated ReLU into the diagonal layer of UDV. When the non-negativity constraints are applied on the diagonal layer, we refer to the model as UDV-ReLU; otherwise, it is called UDV-ReLU-s.

We conducted a preliminary experiment to verify the feasibility of incorporating ReLU into the UDV, leaving a comprehensive study to future work. We derived the optimizers and learning rates from [Tables SM2 to SM5](#), but only used the HPART dataset for regression and the MNIST for classification.

[Figure SM17](#) and [Figure SM18](#) showed that UDV-ReLU and UDV-ReLU-s exhibit a similar (or even more pronounced) decaying pattern in singular values as observed in the proposed UDV. The ‘stair-step’ accuracy curve was also observed in these models.

B.5 Comparison of UDV and Three-Layer Fully Connected Networks

We extend the experiments to compare the UDV framework with three-layer fully connected neural networks. To highlight the critical role of the UDV structure and its constraints, we include the following models in the comparison: the proposed UDV model, a model based on the UDV structure but without the constraints (UDV unconstrained), a fully connected three-layer neural network (UFV), and the standard UV model as the baseline.

The results, also included in [Tables SM2 to SM5](#), are shown in [Figure SM19](#) and [Figure SM20](#). These findings demonstrate that the singular value decay in UDV unconstrained, UFV, and UV is significantly slower than in the proposed UDV framework. This underscores the critical role of the diagonal layer and constraints in facilitating low-rank solution identification within the proposed structure.

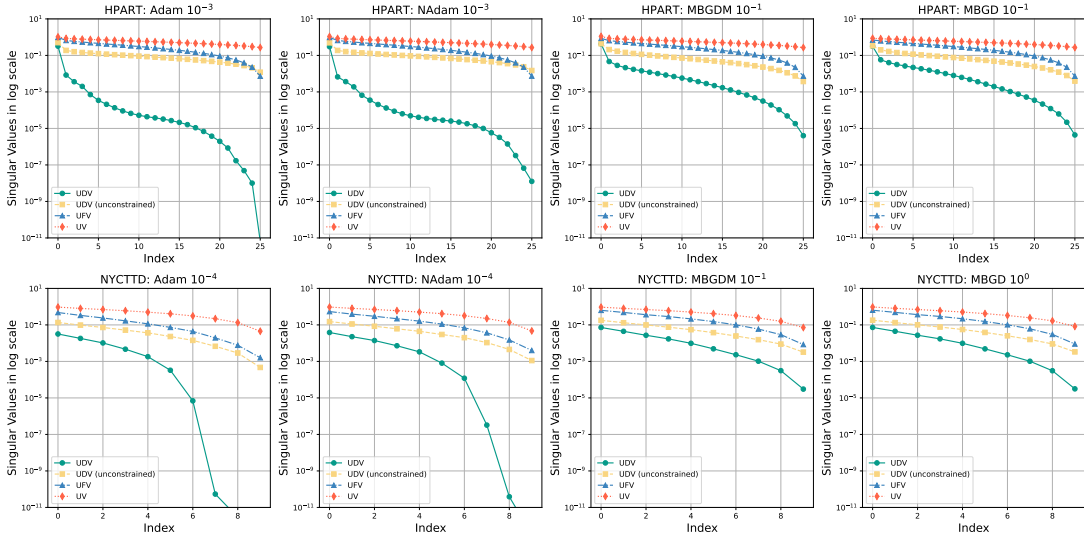


Figure SM19: Comparison of singular value spectrum among UDV, UDV (unconstrained),UFV and UV on the regression tasks.

B.6 Comparing the Effects of UDV and Weight Decay Regularization

We conducted a preliminary experiment to compare the singular value decay in two-layer (UV) and three-layer (UFV) fully connected network blocks with weight decay regularization to that observed in the UDV framework. We focused on the regression task with the HPART dataset. For the regularization parameter (γ), we tested values 10^{-6} , 10^{-5} , \dots , 10^{-1} .

Increasing γ led to a faster decay in the singular value spectrum but at the cost of higher training and validation losses. [Figure SM21](#) illustrates an example where we selected the largest γ values for which the validation loss remained within 10% of the UDV baseline. The resulting singular value decay in the UV and UFV models was less pronounced than in the UDV model. Further increasing γ to match or exceed the spectral decay of the UDV model resulted in significantly worse validation loss compared to the UDV network. The complete results are presented in [Figures SM22](#) and [SM23](#).

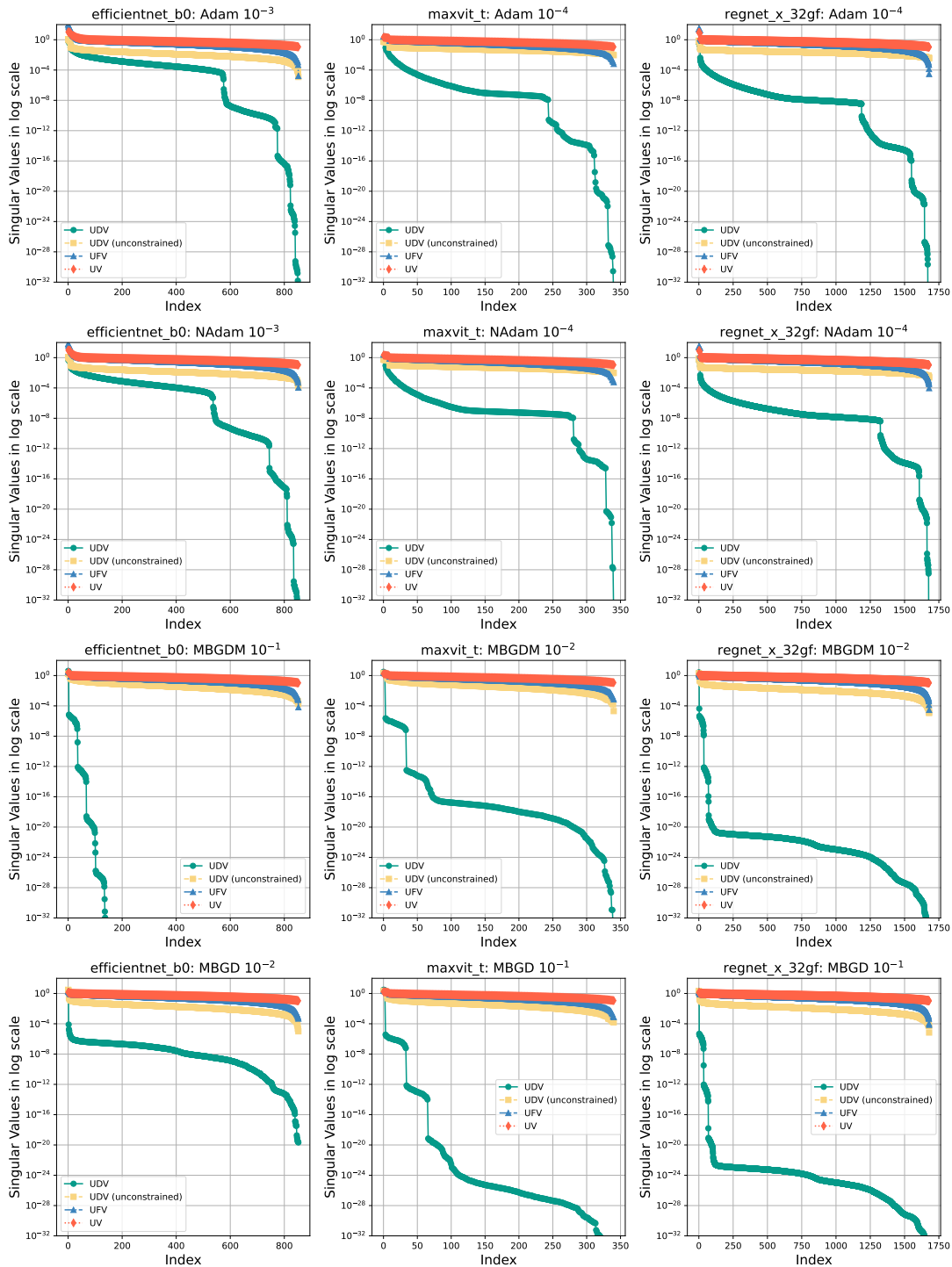


Figure SM20: Comparison of singular value spectrum among UDV, UDV (unconstrained), UFV and UV on the classification datasets (MNIST).

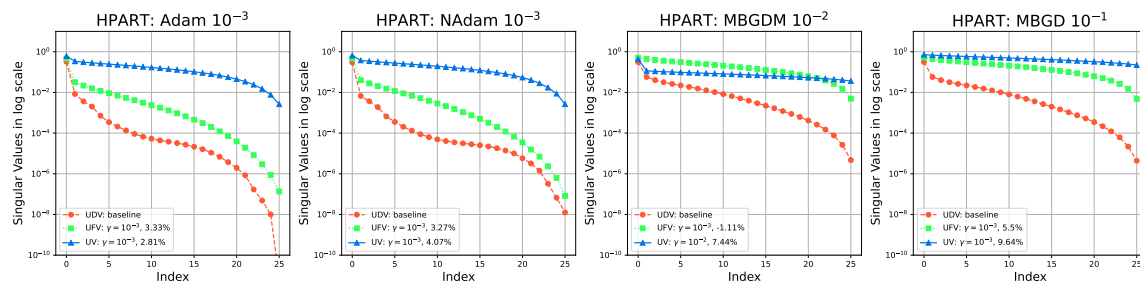


Figure SM21: Comparison of singular value spectrum among the proposed UDV, UFV and UV (with weight decay) on the HPART dataset. In addition to the UDV baseline, the UFV and UV models include the regularization parameter γ and the relative change in validation performance. The relative change is defined as $\left(\frac{\text{loss}_{\text{model}} - \text{loss}_{\text{baseline}}}{\text{loss}_{\text{baseline}}} \times 100\%\right)$, representing how much worse the model performs compared to the UDV baseline.

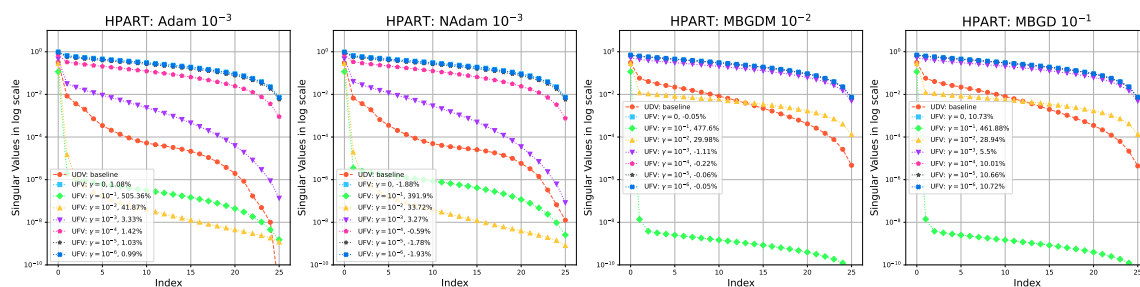


Figure SM22: Extension of Figure SM21. Comparison of singular value spectrum between the proposed UDV and UFV (with weight decay) on the HPART dataset. Regularization parameter $\gamma = 0$ indicates that no weight decay is applied.

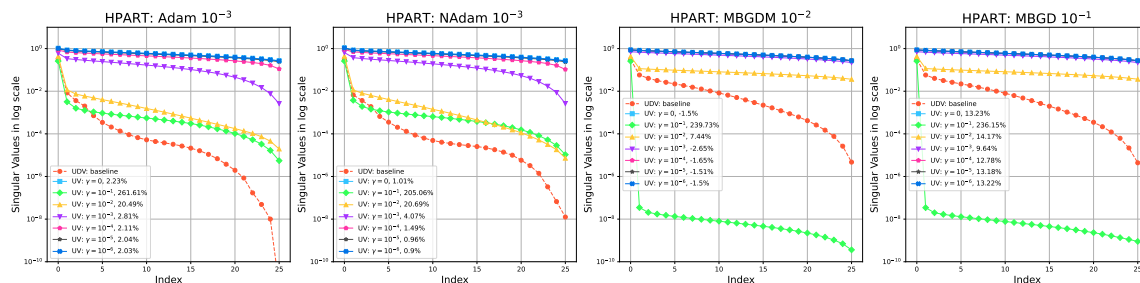


Figure SM23: Extension of Figure SM21. Comparison of singular value spectrum between the proposed UDV and UV (with weight decay) on the HPART dataset. Regularization parameter $\gamma = 0$ indicates that no weight decay is applied.

Table SM2: Experiments using Adam optimizer. Not applicable or results with obvious oscillations or divergence are denoted as ‘-’.

Tasks		Regression (Test Loss)		Classification (Test Accuracy)		
Dataset	HPART	NYCTTD	MNIST			
(Transferred model)	($\times 10^{-3}$)	($\times 10^{-6}$)	(MaxVit-T [M] EfficientNet-B0 [E] RegNetX-32GF [R])	($\times 100\%$)		
LR: 10^{-6}	-	-	UDV: - UDV-s: - UDV-v1: 99.56 UDV-v2: 99.53 UDV-ReLU: - UDV(unconstrained): 99.53 UFV: 99.53 UV-ReLU: 99.59 UV: 99.54 M: 99.42	UDV: - UDV-s: - UDV-v1: - UDV-v2: - UDV-ReLU: - UDV(unconstrained): - UFV: 99.25 UV-ReLU: 99.29 UV: 99.24 E: 98.67	UDV: - UDV-s: - UDV-v1: 99.46 UDV-v2: 99.48 UDV-ReLU: - UDV(unconstrained): 99.48 UFV: 99.38 UV-ReLU: 99.41 UV: 99.36 R: 99.32	
LR: 10^{-5}	-	-	UDV: - UDV-s: - UDV-v1: 99.61 UDV-v2: 99.58 UDV-ReLU: - UDV(unconstrained): 99.62 UFV: 99.60 UV-ReLU: 99.57 UV: 99.61 M: 99.59	UDV: - UDV-s: - UDV-v1: 99.49 UDV-v2: 99.53 UDV-ReLU: - UDV(unconstrained): 99.54 UFV: 99.43 UV-ReLU: 99.52 UV: 99.52 E: 99.51	UDV: - UDV-s: - UDV-v1: 99.58 UDV-v2: 99.50 UDV-ReLU: - UDV(unconstrained): 99.50 UFV: 99.58 UV-ReLU: 99.59 UV: 99.57 R: 99.59	
LR: 10^{-4}	UDV: 2.304 UDV-s: 1.912 UDV-v1: 1.823 UDV-v2: 1.738 UDV-ReLU: 2.731 UDV(unconstrained): 1.738 UFV: 1.351 UV-ReLU: 1.376 UV: 1.475	UDV: 5.248 UDV-s: 5.248 UDV-v1: 5.248 UDV-v2: 5.250 UDV-ReLU: 5.251 UDV(unconstrained): 5.250 UFV: 5.254 UV-ReLU: 5.263 UV: 5.275	UDV: 99.66 UDV-s: 99.58 UDV-v1: 99.65 UDV-v2: 99.69 UDV-ReLU: 99.63 UDV(unconstrained): 99.66 UFV: 99.69 UV-ReLU: 99.63 UV: 99.64 M: 99.65	UDV: - UDV-s: - UDV-v1: 99.63 UDV-v2: 99.58 UDV-ReLU: - UDV(unconstrained): 99.63 UFV: 99.59 UV-ReLU: 99.54 UV: 99.56 E: 99.60	UDV: 99.55 UDV-s: 99.55 UDV-v1: 99.56 UDV-v2: 99.68 UDV-ReLU: - UDV(unconstrained): 99.59 UFV: 99.67 UV-ReLU: 99.64 UV: 99.60 R: 99.59	
LR: 10^{-3}	UDV: 1.304 UDV-s: 1.316 UDV-v1: 1.267 UDV-v2: 1.268 UDV-ReLU: 1.320 UDV(unconstrained): 1.268 UFV: 1.318 UV-ReLU: 1.167 UV: 1.333	UDV: 5.248 UDV-s: 5.248 UDV-v1: 5.248 UDV-v2: 5.248 UDV-ReLU: 5.251 UDV(unconstrained): 5.248 UFV: 5.248 UV-ReLU: 5.306 UV: 5.251	UDV: 99.57 UDV-s: 99.59 UDV-v1: 99.57 UDV-v2: 99.58 UDV-ReLU: 99.51 UDV(unconstrained): 99.52 UFV: 99.59 UV-ReLU: 99.60 UV: 99.60 M: 99.63	UDV: 99.55 UDV-s: 99.59 UDV-v1: 99.59 UDV-v2: 99.57 UDV-ReLU: 99.54 UDV(unconstrained): 99.57 UFV: 99.54 UV-ReLU: 99.49 UV: 99.60 E: 99.61	UDV: 99.50 UDV-s: 99.49 UDV-v1: 99.47 UDV-v2: 99.47 UDV-ReLU: 99.42 UDV(unconstrained): 99.58 UFV: 99.41 UV-ReLU: 99.66 UV: 99.46 R: 99.49	
LR: 10^{-2}	UDV: 1.877 UDV-s: 1.998 UDV-v1: 1.409 UDV-v2: 1.500 UDV-ReLU: 1.699 UDV(unconstrained): 1.402 UFV: 1.483 UV-ReLU: 1.467 UV: 1.430	UDV: 5.257 UDV-s: 5.258 UDV-v1: 5.256 UDV-v2: 5.257 UDV-ReLU: 5.323 UDV(unconstrained): 5.263 UFV: 7.048 UV-ReLU: 5.323 UV: 7.369	UDV: - UDV-s: - UDV-v1: - UDV-v2: - UDV-ReLU: - UDV(unconstrained): - UFV: - UV-ReLU: - UV: - M: -	UDV: 99.34 UDV-s: 99.56 UDV-v1: 99.48 UDV-v2: 99.44 UDV-ReLU: 96.95 UDV(unconstrained): 99.52 UFV: - UV-ReLU: 99.37 UV: 99.32 E: 98.42	UDV: 99.53 UDV-s: 99.43 UDV-v1: 99.35 UDV-v2: 99.28 UDV-ReLU: 99.37 UDV(unconstrained): 99.10 UFV: - UV-ReLU: 99.32 UV: 98.90 R: 99.39	
LR: 10^{-1}	UDV: 4.188 UDV-s: - UDV-v1: - UDV-v2: - UDV-ReLU: 18.26 UDV(unconstrained): - UFV: 1.745 UV-ReLU: 42.01 UV: 1.614	UDV: 5.321 UDV-s: 114.6 UDV-v1: 23.12 UDV-v2: 21.22 UDV-ReLU: 5.323 UDV(unconstrained): 126.1 UFV: - UV-ReLU: 5.323 UV: -	UDV: - UDV-s: - UDV-v1: - UDV-v2: - UDV-ReLU: - UDV(unconstrained): - UFV: - UV-ReLU: - UV: - M: -	UDV: 99.05 UDV-s: 95.62 UDV-v1: - UDV-v2: - UDV-ReLU: - UDV(unconstrained): - UFV: - UV-ReLU: - UV: 97.69 E: 99.10	UDV: 97.54 UDV-s: 99.31 UDV-v1: - UDV-v2: - UDV-ReLU: - UDV(unconstrained): - UFV: - UV-ReLU: - UV: - R: 99.22	
LR: 10^0	UDV: 38.71 UDV-s: - UDV-v1: 2.413 UDV-v2: 4.633 UDV-ReLU: 48.62 UDV(unconstrained): 14.05 UFV: - UV-ReLU: 48.24 UV: -	UDV: 5.327 UDV-s: - UDV-v1: 16.19 UDV-v2: - UDV-ReLU: 5.323 UDV(unconstrained): - UFV: - UV-ReLU: 5.323 UV: -	UDV: - UDV-s: - UDV-v1: - UDV-v2: - UDV-ReLU: - UDV(unconstrained): - UFV: - UV-ReLU: - UV: - M: -	UDV: 99.10 UDV-s: - UDV-v1: - UDV-v2: - UDV-ReLU: - UDV(unconstrained): - UFV: - UV-ReLU: - UV: - E: -	UDV: - UDV-s: - UDV-v1: - UDV-v2: - UDV-ReLU: - UDV(unconstrained): - UFV: - UV-ReLU: - UV: - R: 95.65	
LR: 2×10^0	UDV: 60.46 UDV-s: - UDV-v1: 6.651 UDV-v2: 7.366 UDV-ReLU: 48.62 UDV(unconstrained): - UFV: - UV-ReLU: 49.43 UV: -	UDV: 5.322 UDV-s: - UDV-v1: - UDV-v2: - UDV-ReLU: 5.323 UDV(unconstrained): - UFV: - UV-ReLU: 5.323 UV: -	-	-	-	
LR: 3×10^0	UDV: 106.9 UDV-s: - UDV-v1: 6.606 UDV-v2: 7.398 UDV-ReLU: 48.62 UDV(unconstrained): - UFV: - UV-ReLU: 48.50 UV: -	UDV: 5.335 UDV-s: - UDV-v1: 6.380 UDV-v2: - UDV-ReLU: 5.323 UDV(unconstrained): - UFV: - UV-ReLU: 5.323 UV: -	-	-	-	
LR: 5×10^0	-	-	-	-	-	

Table SM3: Experiments using NAdam optimizer. Not applicable or results with obvious oscillations or divergence are denoted as ‘-’.

Tasks		Regression (Test Loss)		Classification (Test Accuracy)		
Dataset	HPART	NYCTTD	MNIST			
(Transferred model)	($\times 10^{-3}$)	($\times 10^{-6}$)	(MaxVit-T [M] EfficientNet-B0 [E] RegNetX-32GF [R])	(×100%)		
LR: 10^{-6}	-	-	UDV: - UDV-s: - UDV-v1: 99.56 UDV-v2: 99.53 UDV-ReLU: - UDV(unconstrained): 99.53 UFV: 99.54 UV-ReLU: 99.59 UV: 99.53 M: 99.41	UDV: - UDV-s: - UDV-v1: - UDV-v2: - UDV-ReLU: - UDV(unconstrained): - UFV: 99.26 UV-ReLU: 99.30 UV: 99.24 E: 98.67	UDV: - UDV-s: - UDV-v1: 99.49 UDV-v2: 99.46 UDV-ReLU: - UDV(unconstrained): 99.46 UFV: 99.32 UV-ReLU: 99.40 UV: 99.32 R: 99.37	
LR: 10^{-5}	-	-	UDV: - UDV-s: - UDV-v1: 99.63 UDV-v2: 99.59 UDV-ReLU: - UDV(unconstrained): 99.60 UFV: 99.62 UV-ReLU: 99.61 UV: 99.63 M: 99.62	UDV: - UDV-s: - UDV-v1: 99.50 UDV-v2: 99.52 UDV-ReLU: - UDV(unconstrained): 99.52 UFV: 99.43 UV-ReLU: 99.51 UV: 99.52 E: 99.50	UDV: - UDV-s: - UDV-v1: 99.66 UDV-v2: 99.56 UDV-ReLU: - UDV(unconstrained): 99.56 UFV: 99.54 UV-ReLU: 99.59 UV: 99.61 R: 99.67	
LR: 10^{-4}	UDV: 2.312 UDV-s: 1.916 UDV-v1: 1.837 UDV-v2: 1.752 UDV-ReLU: 2.665 UDV(unconstrained): 1.752 UFV: 1.381 UV-ReLU: 1.398 UV: 1.512	UDV: 5.248 UDV-s: 5.248 UDV-v1: 5.248 UDV-v2: 5.249 UDV-ReLU: 5.251 UDV(unconstrained): 5.249 UFV: 5.256 UV-ReLU: 5.258 UV: 5.275	UDV: 99.67 UDV-s: 99.62 UDV-v1: 99.67 UDV-v2: 99.61 UDV-ReLU: 99.63 UDV(unconstrained): 99.62 UFV: 99.68 UV-ReLU: 99.68 UV: 99.65 M: 99.59	UDV: - UDV-s: - UDV-v1: 99.60 UDV-v2: 99.66 UDV-ReLU: - UDV(unconstrained): 99.60 UFV: 99.54 UV-ReLU: 99.53 UV: 99.53 E: 99.65	UDV: 99.52 UDV-s: 99.55 UDV-v1: 99.69 UDV-v2: 99.72 UDV-ReLU: 99.46 UDV(unconstrained): 99.63 UFV: 99.55 UV-ReLU: 99.63 UV: 99.64 R: 99.64	
LR: 10^{-3}	UDV: 1.638 UDV-s: 1.691 UDV-v1: 1.418 UDV-v2: 1.440 UDV-ReLU: 1.504 UDV(unconstrained): 1.437 UFV: 1.607 UV-ReLU: 1.367 UV: 1.654	UDV: 5.248 UDV-s: 5.248 UDV-v1: 5.248 UDV-v2: 5.248 UDV-ReLU: 5.251 UDV(unconstrained): 5.248 UFV: 5.248 UV-ReLU: 5.249 UV: 5.254	UDV: 99.53 UDV-s: 99.56 UDV-v1: 99.54 UDV-v2: 99.61 UDV-ReLU: 99.55 UDV(unconstrained): 99.66 UFV: 99.57 UV-ReLU: 99.63 UV: 99.59 M: 99.58	UDV: 97.56 UDV-s: 99.61 UDV-v1: 99.60 UDV-v2: 99.55 UDV-ReLU: 99.50 UDV(unconstrained): 99.55 UFV: 99.28 UV-ReLU: 99.55 UV: 99.55 E: 99.58	UDV: 99.45 UDV-s: 99.45 UDV-v1: 99.43 UDV-v2: 99.46 UDV-ReLU: 99.47 UDV(unconstrained): 99.50 UFV: 99.27 UV-ReLU: 99.53 UV: 99.42 R: 99.65	
LR: 10^{-2}	UDV: 3.396 UDV-s: 3.287 UDV-v1: 2.297 UDV-v2: 2.315 UDV-ReLU: 2.403 UDV(unconstrained): 1.884 UFV: - UV-ReLU: 1.954 UV: -	UDV: 5.258 UDV-s: 6.918 UDV-v1: 5.276 UDV-v2: 5.253 UDV-ReLU: 5.323 UDV(unconstrained): 5.253 UFV: 25.24 UV-ReLU: 5.323 UV: 6.262	UDV: - UDV-s: - UDV-v1: - UDV-v2: - UDV-ReLU: - UDV(unconstrained): - UFV: - UV-ReLU: - UV: - M: -	UDV: 99.35 UDV-s: - UDV-v1: 99.31 UDV-v2: 99.01 UDV-ReLU: 99.42 UDV(unconstrained): 98.78 UFV: - UV-ReLU: 98.87 UV: 98.60 E: 99.26	UDV: 97.12 UDV-s: 99.28 UDV-v1: 99.37 UDV-v2: 99.38 UDV-ReLU: 99.49 UDV(unconstrained): 99.38 UFV: - UV-ReLU: 99.28 UV: 98.91 R: 99.59	
LR: 10^{-1}	UDV: 13.69 UDV-s: - UDV-v1: - UDV-v2: - UDV-ReLU: 48.62 UDV(unconstrained): - UFV: 4.918 UV-ReLU: 41.61 UV: 1.863	UDV: 5.323 UDV-s: - UDV-v1: 6.627 UDV-v2: - UDV-ReLU: 5.323 UDV(unconstrained): - UFV: - UV-ReLU: 5.323 UV: -	UDV: - UDV-s: - UDV-v1: - UDV-v2: - UDV-ReLU: - UDV(unconstrained): - UFV: - UV-ReLU: - UV: - M: -	UDV: - UDV-s: - UDV-v1: - UDV-v2: - UDV-ReLU: - UDV(unconstrained): - UFV: - UV-ReLU: - UV: 97.54 E: 98.75	UDV: - UDV-s: - UDV-v1: - UDV-v2: - UDV-ReLU: - UDV(unconstrained): - UFV: - UV-ReLU: - UV: - R: 99.19	
LR: 10^0	UDV: - UDV-s: - UDV-v1: 5.649 UDV-v2: 2.317 UDV-ReLU: 48.62 UDV(unconstrained): - UFV: - UV-ReLU: 45.77 UV: -	UDV: 5.328 UDV-s: 53.70 UDV-v1: 19.52 UDV-v2: - UDV-ReLU: 5.323 UDV(unconstrained): - UFV: - UV-ReLU: 5.323 UV: -	UDV: - UDV-s: - UDV-v1: - UDV-v2: - UDV-ReLU: - UDV(unconstrained): - UFV: - UV-ReLU: - UV: - M: -	UDV: - UDV-s: - UDV-v1: - UDV-v2: - UDV-ReLU: - UDV(unconstrained): - UFV: - UV-ReLU: - UV: - E: -	UDV: - UDV-s: - UDV-v1: - UDV-v2: - UDV-ReLU: - UDV(unconstrained): - UFV: - UV-ReLU: - UV: - R: -	
LR: 2×10^0	UDV: - UDV-s: - UDV-v1: 3.075 UDV-v2: 2.828 UDV-ReLU: 48.62 UDV(unconstrained): - UFV: - UV-ReLU: 59.82 UV: -	UDV: 5.377 UDV-s: - UDV-v1: 6.011 UDV-v2: - UDV-ReLU: 5.323 UDV(unconstrained): - UFV: - UV-ReLU: 5.323 UV: -	-	-	-	
LR: 3×10^0	UDV: - UDV-s: - UDV-v1: 3.882 UDV-v2: 3.128 UDV-ReLU: 48.62 UDV(unconstrained): - UFV: - UV-ReLU: - UV: -	UDV: 5.401 UDV-s: - UDV-v1: 15.27 UDV-v2: - UDV-ReLU: 5.323 UDV(unconstrained): - UFV: - UV-ReLU: 5.323 UV: -	-	-	-	
LR: 5×10^0	-	-	-	-	-	

Table SM4: Experiments using MBGD optimizer. Not applicable or results with obvious oscillations or divergence are denoted as ‘-’.

Tasks		Regression (Test Loss)		Classification (Test Accuracy)		
Dataset	HPART	NYCTTD	MNIST			
(Transferred model)	($\times 10^{-3}$)	($\times 10^{-6}$)	(MaxVit-T [M] EffcientNet-B0 [E] RegNetX-32GF [R])	(×100%)		
LR: 10^{-6}	-	-	-	-	-	
LR: 10^{-5}	-	-	-	-	-	
LR: 10^{-4}	UDV: 46.90	UDV: 26.60	-	-	-	
	UDV-s: 45.43	UDV-s: 40.06	-	-	-	
	UDV-v1: 46.01	UDV-v1: 49.35	-	-	-	
	UDV-v2: 44.35	UDV-v2: 83.91	-	-	-	
	UDV-ReLU: 47.88	UDV-ReLU: 20.56	-	-	-	
	UDV(unconstrained): 44.35	UDV(unconstrained): 83.91	-	-	-	
	UFV: 11.77	UFV: 86.68	-	-	-	
UV-ReLU: 12.59	UV-ReLU: -	-	-	-		
UV: 11.98	UV: 71.72	-	-	-		
LR: 10^{-3}	UDV: 30.38	UDV: 9.407	UDV: -	UDV: -	UDV: -	
	UDV-s: 21.39	UDV-s: 10.29	UDV-s: -	UDV-s: -	UDV-s: -	
	UDV-v1: 23.65	UDV-v1: 10.83	UDV-v1: 98.44	UDV-v1: -	UDV-v1: -	
	UDV-v2: 15.77	UDV-v2: 12.56	UDV-v2: 98.32	UDV-v2: -	UDV-v2: -	
	UDV-ReLU: 39.89	UDV-ReLU: 7.231	UDV-ReLU: -	UDV-ReLU: -	UDV-ReLU: -	
	UDV(unconstrained): 15.77	UDV(unconstrained): 12.56	UDV(unconstrained): 98.27	UDV(unconstrained): -	UDV(unconstrained): -	
	UFV: 6.719	UFV: 8.236	UFV: 99.34	UFV: 98.15	UFV: 99.20	
	UV-ReLU: 6.478	UV-ReLU: 12.67	UV-ReLU: 99.24	UV-ReLU: 98.48	UV-ReLU: 99.16	
	UV: 6.345	UV: 6.763	UV: 99.19	UV: 98.55	UV: 99.17	
			M: 99.29	E: 98.74	R: 99.16	
LR: 10^{-2}	UDV: 6.030	UDV: 5.465	UDV: 99.38	UDV: -	UDV: 99.40	
	UDV-s: 6.014	UDV-s: 5.421	UDV-s: 99.32	UDV-s: -	UDV-s: 99.46	
	UDV-v1: 6.125	UDV-v1: 5.514	UDV-v1: 99.47	UDV-v1: 98.62	UDV-v1: 99.37	
	UDV-v2: 5.877	UDV-v2: 5.532	UDV-v2: 99.50	UDV-v2: 98.97	UDV-v2: 99.34	
	UDV-ReLU: 6.234	UDV-ReLU: 5.431	UDV-ReLU: 99.53	UDV-ReLU: -	UDV-ReLU: 99.47	
	UDV(unconstrained): 5.877	UDV(unconstrained): 5.532	UDV(unconstrained): 99.58	UDV(unconstrained): 98.40	UDV(unconstrained): 99.34	
	UFV: 5.575	UFV: 5.293	UFV: 99.53	UFV: 99.05	UFV: 99.36	
	UV-ReLU: 2.253	UV-ReLU: 5.521	UV-ReLU: 99.53	UV-ReLU: 99.31	UV-ReLU: 99.31	
	UV: 2.251	UV: 5.296	UV: 99.50	UV: 99.24	UV: 99.38	
			M: 99.59	E: 99.43	R: 99.44	
LR: 10^{-1}	UDV: 1.398	UDV: 5.253	UDV: 99.59	UDV: -	UDV: 99.51	
	UDV-s: 1.407	UDV-s: 5.250	UDV-s: 99.38	UDV-s: 99.36	UDV-s: 99.57	
	UDV-v1: 1.556	UDV-v1: 5.256	UDV-v1: 99.61	UDV-v1: 99.43	UDV-v1: 99.60	
	UDV-v2: 1.565	UDV-v2: 5.252	UDV-v2: 99.60	UDV-v2: 99.53	UDV-v2: 99.62	
	UDV-ReLU: 1.379	UDV-ReLU: 5.277	UDV-ReLU: 99.65	UDV-ReLU: 95.21	UDV-ReLU: -	
	UDV(unconstrained): 1.565	UDV(unconstrained): 5.252	UDV(unconstrained): 99.59	UDV(unconstrained): 95.29	UDV(unconstrained): 99.61	
	UFV: 1.548	UFV: 5.255	UFV: 99.61	UFV: 99.55	UFV: 99.59	
	UV-ReLU: 1.493	UV-ReLU: 5.323	UV-ReLU: 99.60	UV-ReLU: 99.52	UV-ReLU: 99.59	
	UV: 1.583	UV: 5.291	UV: 99.63	UV: 99.55	UV: 98.56	
			M: 99.62	E: 99.67	R: 99.63	
LR: 10^0	UDV: 3.076	UDV: 5.248	UDV: -	UDV: -	UDV: -	
	UDV-s: 2.870	UDV-s: 5.248	UDV-s: -	UDV-s: -	UDV-s: -	
	UDV-v1: 1.935	UDV-v1: 5.249	UDV-v1: -	UDV-v1: 99.65	UDV-v1: 99.67	
	UDV-v2: 1.830	UDV-v2: 5.248	UDV-v2: -	UDV-v2: 99.59	UDV-v2: 99.69	
	UDV-ReLU: 4.573	UDV-ReLU: 5.261	UDV-ReLU: -	UDV-ReLU: -	UDV-ReLU: -	
	UDV(unconstrained): 1.810	UDV(unconstrained): 5.248	UDV(unconstrained): -	UDV(unconstrained): 99.62	UDV(unconstrained): 99.57	
	UFV: -	UFV: 5.256	UFV: -	UFV: -	UFV: -	
	UV-ReLU: 48.62	UV-ReLU: 5.271	UV-ReLU: -	UV-ReLU: 99.64	UV-ReLU: 99.73	
	UV: -	UV: -	UV: -	UV: -	UV: 99.66	
			M: -	E: 99.55	R: 99.66	
LR: 2×10^0	UDV: 6.244	UDV: 5.248	UDV: -	UDV: -	UDV: -	
	UDV-s: 48.63	UDV-s: 5.248	UDV-s: -	UDV-s: -	UDV-s: -	
	UDV-v1: 2.559	UDV-v1: 5.249	UDV-v1: -	UDV-v1: 98.37	UDV-v1: 99.66	
	UDV-v2: -	UDV-v2: 5.249	UDV-v2: -	UDV-v2: 99.66	UDV-v2: 99.55	
	UDV-ReLU: 47.50	UDV-ReLU: 5.259	UDV-ReLU: -	UDV-ReLU: -	UDV-ReLU: -	
	UDV(unconstrained): -	UDV(unconstrained): 5.249	UDV(unconstrained): -	UDV(unconstrained): -	UDV(unconstrained): -	
	UFV: -	UFV: -	UFV: -	UFV: -	UFV: -	
	UV-ReLU: 48.63	UV-ReLU: 5.293	UV-ReLU: -	UV-ReLU: -	UV-ReLU: 99.58	
	UV: -	UV: -	UV: -	UV: -	UV: 99.57	
			M: -	E: 98.88	R: 99.56	
LR: 3×10^0	UDV: -	UDV: 5.248	UDV: -	UDV: -	UDV: -	
	UDV-s: -	UDV-s: 5.248	UDV-s: -	UDV-s: -	UDV-s: -	
	UDV-v1: -	UDV-v1: 5.249	UDV-v1: -	UDV-v1: 99.07	UDV-v1: 99.48	
	UDV-v2: -	UDV-v2: 5.249	UDV-v2: -	UDV-v2: -	UDV-v2: 99.65	
	UDV-ReLU: 48.62	UDV-ReLU: 5.257	UDV-ReLU: -	UDV-ReLU: -	UDV-ReLU: -	
	UDV(unconstrained): -	UDV(unconstrained): 5.250	UDV(unconstrained): -	UDV(unconstrained): -	UDV(unconstrained): -	
	UFV: -	UFV: -	UFV: -	UFV: -	UFV: -	
	UV-ReLU: 48.62	UV-ReLU: 5.296	UV-ReLU: -	UV-ReLU: -	UV-ReLU: 99.57	
	UV: -	UV: -	UV: -	UV: -	UV: -	
			M: -	E: 99.26	R: 99.57	
LR: 5×10^0	UDV: -	UDV: -	UDV: -	UDV: -	UDV: -	
	UDV-s: -	UDV-s: -	UDV-s: -	UDV-s: -	UDV-s: -	
	UDV-v1: -	UDV-v1: -	UDV-v1: -	UDV-v1: -	UDV-v1: 99.55	
	UDV-v2: -	UDV-v2: -	UDV-v2: -	UDV-v2: -	UDV-v2: 99.41	
	UDV-ReLU: -	UDV-ReLU: -	UDV-ReLU: -	UDV-ReLU: -	UDV-ReLU: -	
	UDV(unconstrained): -	UDV(unconstrained): -	UDV(unconstrained): -	UDV(unconstrained): -	UDV(unconstrained): -	
	UFV: -	UFV: -	UFV: -	UFV: -	UFV: -	
	UV-ReLU: -	UV-ReLU: -	UV-ReLU: -	UV-ReLU: -	UV-ReLU: 99.42	
	UV: -	UV: -	UV: -	UV: -	UV: -	
			M: -	E: 99.33	R: 99.55	

Table SM5: Experiments using MBGDM optimizer. Not applicable or results with obvious oscillations or divergence are denoted as ‘-’.

Tasks		Regression (Test Loss)		Classification (Test Accuracy)		
Dataset	HPART	NYCTTD	MNIST			
(Transferred model)	($\times 10^{-3}$)	($\times 10^{-6}$)	(MaxVit-T [M] EffcientNet-B0 [E] RegNetX-32GF [R])	(×100%)		
LR: 10^{-6}	-	-	-	-	-	
LR: 10^{-5}	-	-	-	-	-	
LR: 10^{-4}	UDV: 30.52	UDV: 9.413	-	-	-	
	UDV-s: 21.50	UDV-s: 10.29	-	-	-	
	UDV-v1: 23.79	UDV-v1: 10.85	-	-	-	
	UDV-v2: 15.84	UDV-v2: 12.59	-	-	-	
	UDV-ReLU: 40.00	UDV-ReLU: 7.224	-	-	-	
	UDV(unconstrained): 15.84	UDV(unconstrained): 12.59	-	-	-	
	UFV: 6.729	UFV: 8.288	-	-	-	
UV-ReLU: 6.488	UV-ReLU: 12.68	-	-	-		
UV: 6.348	UV: 6.776	-	-	-		
LR: 10^{-3}	UDV: 6.105	UDV: 5.457	UDV: 99.26	UDV: -	UDV: 99.50	
	UDV-s: 6.080	UDV-s: 5.412	UDV-s: 99.38	UDV-s: -	UDV-s: 99.43	
	UDV-v1: 6.178	UDV-v1: 5.516	UDV-v1: 99.39	UDV-v1: 99.00	UDV-v1: 99.39	
	UDV-v2: 5.929	UDV-v2: 5.534	UDV-v2: 99.52	UDV-v2: 99.05	UDV-v2: 99.37	
	UDV-ReLU: 6.341	UDV-ReLU: 5.431	UDV-ReLU: -	UDV-ReLU: -	UDV-ReLU: -	
	UDV(unconstrained): 5.929	UDV(unconstrained): 5.534	UDV(unconstrained): 99.51	UDV(unconstrained): 99.08	UDV(unconstrained): 99.40	
	UFV: 2.590	UFV: 5.294	UFV: 99.56	UFV: 99.18	UFV: 99.38	
	UV-ReLU: 2.529	UV-ReLU: 5.520	UV-ReLU: 99.46	UV-ReLU: 99.37	UV-ReLU: 99.36	
	UV: 2.252	UV: 5.296	UV: 99.54	UV: 99.36	UV: 99.30	
			M: 99.58	E: 99.45	R: 99.41	
LR: 10^{-2}	UDV: 1.357	UDV: 5.253	UDV: 99.67	UDV: 99.48	UDV: 99.74	
	UDV-s: 1.388	UDV-s: 5.250	UDV-s: 99.38	UDV-s: 99.60	UDV-s: 99.72	
	UDV-v1: 1.554	UDV-v1: 5.256	UDV-v1: 99.63	UDV-v1: 99.54	UDV-v1: 99.61	
	UDV-v2: 1.569	UDV-v2: 5.252	UDV-v2: 99.60	UDV-v2: 99.59	UDV-v2: 99.67	
	UDV-ReLU: 1.312	UDV-ReLU: 5.276	UDV-ReLU: 99.62	UDV-ReLU: 99.54	UDV-ReLU: 99.65	
	UDV(unconstrained): 1.569	UDV(unconstrained): 5.252	UDV(unconstrained): 99.59	UDV(unconstrained): 99.55	UDV(unconstrained): 99.63	
	UFV: 1.357	UFV: 5.254	UFV: 99.65	UFV: 99.50	UFV: 99.66	
	UV-ReLU: 1.314	UV-ReLU: 5.267	UV-ReLU: 99.63	UV-ReLU: 99.53	UV-ReLU: 99.61	
	UV: 1.337	UV: 5.279	UV: 99.69	UV: 99.50	UV: 99.53	
			M: 99.64	E: 99.59	R: 99.60	
LR: 10^{-1}	UDV: 1.345	UDV: 5.248	UDV: 99.61	UDV: 99.63	UDV: 99.60	
	UDV-s: 1.339	UDV-s: 5.248	UDV-s: 99.60	UDV-s: 99.63	UDV-s: 99.57	
	UDV-v1: 1.313	UDV-v1: 5.249	UDV-v1: 99.65	UDV-v1: 99.64	UDV-v1: 99.71	
	UDV-v2: 1.302	UDV-v2: 5.248	UDV-v2: 99.68	UDV-v2: 99.66	UDV-v2: 99.67	
	UDV-ReLU: 1.318	UDV-ReLU: 5.259	UDV-ReLU: -	UDV-ReLU: 99.61	UDV-ReLU: -	
	UDV(unconstrained): 1.302	UDV(unconstrained): 2.248	UDV(unconstrained): 99.70	UDV(unconstrained): 99.59	UDV(unconstrained): 99.67	
	UFV: 1.358	UFV: 5.251	UFV: -	UFV: 99.68	UFV: 99.63	
	UV-ReLU: 1.244	UV-ReLU: 5.264	UV-ReLU: 99.63	UV-ReLU: 99.68	UV-ReLU: 99.66	
UV: -	UV: 5.259	UV: -	UV: 99.59	UV: 99.56		
		M: -	E: 99.63	R: 99.67		
LR: 10^0	UDV: 123.6	UDV: 5.248	UDV: -	UDV: -	UDV: -	
	UDV-s: -	UDV-s: 5.248	UDV-s: -	UDV-s: -	UDV-s: -	
	UDV-v1: -	UDV-v1: 5.249	UDV-v1: -	UDV-v1: 99.54	UDV-v1: 99.52	
	UDV-v2: -	UDV-v2: 5.249	UDV-v2: -	UDV-v2: -	UDV-v2: 99.58	
	UDV-ReLU: 47.03	UDV-ReLU: 5.251	UDV-ReLU: -	UDV-ReLU: -	UDV-ReLU: -	
	UDV(unconstrained): -	UDV(unconstrained): 5.249	UDV(unconstrained): -	UDV(unconstrained): -	UDV(unconstrained): -	
	UFV: -	UFV: -	UFV: -	UFV: -	UFV: -	
	UV-ReLU: 48.62	UV-ReLU: 5.281	UV-ReLU: -	UV-ReLU: -	UV-ReLU: 99.53	
UV: -	UV: -	UV: -	UV: -	UV: -		
		M: -	E: 99.24	R: 99.34		
LR: 2×10^0	UDV: -	UDV: 5.248	UDV: -	UDV: -	UDV: -	
	UDV-s: -	UDV-s: 5.248	UDV-s: -	UDV-s: -	UDV-s: -	
	UDV-v1: -	UDV-v1: 5.249	UDV-v1: -	UDV-v1: -	UDV-v1: 99.31	
	UDV-v2: -	UDV-v2: 5.248	UDV-v2: -	UDV-v2: -	UDV-v2: 99.37	
	UDV-ReLU: 48.62	UDV-ReLU: 5.249	UDV-ReLU: -	UDV-ReLU: -	UDV-ReLU: -	
	UDV(unconstrained): -	UDV(unconstrained): 5.248	UDV(unconstrained): -	UDV(unconstrained): -	UDV(unconstrained): -	
	UFV: -	UFV: -	UFV: -	UFV: -	UFV: -	
	UV-ReLU: 48.62	UV-ReLU: 5.289	UV-ReLU: -	UV-ReLU: -	UV-ReLU: 99.28	
UV: -	UV: -	UV: -	UV: -	UV: -		
		M: -	E: 98.95	R: 99.31		
LR: 3×10^0	UDV: -	UDV: 5.248	UDV: -	UDV: -	UDV: -	
	UDV-s: -	UDV-s: 5.248	UDV-s: -	UDV-s: -	UDV-s: -	
	UDV-v1: -	UDV-v1: 5.248	UDV-v1: -	UDV-v1: -	UDV-v1: -	
	UDV-v2: -	UDV-v2: 5.248	UDV-v2: -	UDV-v2: -	UDV-v2: -	
	UDV-ReLU: 48.62	UDV-ReLU: 5.249	UDV-ReLU: -	UDV-ReLU: -	UDV-ReLU: -	
	UDV(unconstrained): -	UDV(unconstrained): 5.248	UDV(unconstrained): -	UDV(unconstrained): -	UDV(unconstrained): -	
	UFV: -	UFV: -	UFV: -	UFV: -	UFV: -	
	UV-ReLU: 48.62	UV-ReLU: 5.292	UV-ReLU: -	UV-ReLU: -	UV-ReLU: -	
UV: -	UV: -	UV: -	UV: -	UV: -		
		M: -	E: 98.70	R: 99.12		
LR: 5×10^0	UDV: -	UDV: -	UDV: -	UDV: -	UDV: -	
	UDV-s: -	UDV-s: -	UDV-s: -	UDV-s: -	UDV-s: -	
	UDV-v1: -	UDV-v1: -	UDV-v1: -	UDV-v1: 99.55	UDV-v1: 99.55	
	UDV-v2: -	UDV-v2: -	UDV-v2: -	UDV-v2: 99.41	UDV-v2: 99.41	
	UDV-ReLU: -	UDV-ReLU: -	UDV-ReLU: -	UDV-ReLU: -	UDV-ReLU: -	
	UDV(unconstrained): -	UDV(unconstrained): -	UDV(unconstrained): -	UDV(unconstrained): -	UDV(unconstrained): -	
	UFV: -	UFV: -	UFV: -	UFV: -	UFV: -	
	UV-ReLU: -	UV-ReLU: -	UV-ReLU: -	UV-ReLU: -	UV-ReLU: 99.42	
UV: -	UV: -	UV: -	UV: -	UV: -		
		M: -	E: -	R: 99.55		